GigaScience

Multi-dimensional leaf phenotypes reflect root system genotype in grafted grapevine over the growing season

--Manuscript Draft--

Manuscript Number:	GIGA-D-21-00137
Full Title:	Multi-dimensional leaf phenotypes reflect root system genotype in grafted grapevine over the growing season
Article Type:	Research
Funding Information:	National Science Foundation (1546869) — Dr Allison J. Miller
Abstract:	Modern biological approaches generate volumes of multi-dimensional data, offering unprecedented opportunities to address fundamental biological questions previously beyond reach due to small or subtle effects. A fundamental question in plant biology is the extent to which below-ground activity in the root system influences above-ground traits (phenotypes) expressed in the shoot system. Grafting, an ancient agricultural practice that fuses the root system of one individual (the rootstock) with the shoot system of a second, genetically distinct individual (the scion), is a powerful experimental system to understand below-ground effects on above-ground phenotypes. Previous studies on grafted grapevines have detected rootstock influence on scion phenotypes including physiology and berry chemistry; however, the extent of the rootstock's influence on leaves, the photosynthetic engines of the vine, and how those effects changes over the course of a growing season, are still largely unknown. Here, we investigate associations between rootstock genotype and shoot system phenotypes using five multi-dimensional leaf phenotyping modalities measured in a common grafted scion: ionomics, metabolomics, transcriptomics, morphometrics, and physiology. Rootstock influence is ubiquitous but subtle across modalities with the strongest signature of rootstock observed in the leaf ionome. Moreover, we find that the extent of rootstock influence on scion phenotypes and patterns of phenotypic covariation are highly dynamic across the season. These findings substantially expand previously identified patterns to suggest that rootstock influence on scion phenotypes is complex and broad understanding necessitates volumes of multi-dimensional data previously unmet.
Corresponding Author:	Zachary N Harris Saint Louis University SAINT LOUIS, MO UNITED STATES
Corresponding Author Secondary Information:	
Corresponding Author's Institution:	Saint Louis University
Corresponding Author's Secondary Institution:	
First Author:	Zachary N Harris
First Author Secondary Information:	
Order of Authors:	Zachary N Harris
	Mani Awale
	Niyati Bhakta
	Daniel H. Chitwood
	Anne Fennell
	Emma Frawley
	Laura L. Klein
	Laszlo G. Kovacs

	Misha Kwasniewski
	Jason P. Londo
	Qin Ma
	Zoë Migicovsky
	Joel F. Swift
	Allison J. Miller
Order of Authors Secondary Information:	
Additional Information:	
Question	**Response**
Are you submitting this manuscript to a special series or article collection?	No
Experimental design and statistics Full details of the experimental design and statistical methods used should be given in the Methods section, as detailed in our Minimum Standards Reporting Checklist. Information essential to interpreting the data presented should be made available in the figure legends. Have you included all the information requested in your manuscript?	Yes
Resources A description of all resources used, including antibodies, cell lines, animals and software tools, with enough information to allow them to be uniquely identified, should be included in the Methods section. Authors are strongly encouraged to cite Research Resource Identifiers (RRIDs) for antibodies, model organisms and tools, where possible. Have you included the information requested as detailed in our Minimum Standards Reporting Checklist?	Yes
Availability of data and materials All datasets and code on which the	Yes

conclusions of the paper rely must be either included in your submission or deposited in publicly available repositories (where available and ethically appropriate), referencing such data using a unique identifier in the references and in the “Availability of Data and Materials” section of your manuscript. Have you have met the above requirement as detailed in our Minimum Standards Reporting Checklist?	

Multi-dimensional leaf phenotypes reflect root system genotype in grafted grapevine over the growing season

Zachary N. Harris[1,2*] (zachary.n.harris@slu.edu), Mani Awale[3] (maybd@mail.missouri.edu), Niyati Bhakta[1,2] (niyatisbhakta@gmail.com), Daniel H. Chitwood[4,5] (chitwoo9@msu.edu), Anne Fennell[6] (anne.fennell@sdstate.edu), Emma Frawley[1,2] (emma.frawley@wustl.edu), Laura L. Klein[1,2] (laura@leafworks.com), Laszlo G. Kovacs[7] (laszlokovacs@missouristate.edu), Misha Kwasniewski[3] (mtk5407@psu.edu), Jason P. Londo[8] (jason.londo@usda.gov), Qin Ma[9] (qin.ma@osumc.edu), Zoë Migicovsky[10] (zoe.migicovsky@dal.ca), Joel F. Swift[1,2] (joel.swift@slu.edu), and Allison J. Miller[1,2*] (allison.j.miller@slu.edu)

[1]Department of Biology, Saint Louis University, 3507 Laclede Avenue, St. Louis, MO, 63103-2010, USA
[2]Donald Danforth Plant Science Center, 975 North Warson Road, St. Louis, MO, 63132-2918, USA
[3]Division of Plant Sciences, University of Missouri, 135 Eckles Hall, Columbia, MO, 65211, USA
[4]Department of Horticulture, Michigan State University, East Lansing, MI, 48824, USA
[5]Department of Computational Mathematics, Science and Engineering, Michigan State University, East Lansing, MI, 48824, USA
[6]Department of Agronomy, Horticulture & Plant Science, South Dakota State University, Brookings, SD, 57006, USA
[7]Department of Biology, Missouri State University, 901S. National Avenue, Springfield, MO, 65897, USA
[8]United States Department of Agriculture, Agricultural Research Service: Grape Genetics Research Unit, 630 West North Street, Geneva, NY, 14456-1371, USA
[9]Department of Biomedical Informatics, The Ohio State University, 1585 Neil Ave, Columbus, OH, 43210
[10]Department of Plant, Food, and Environmental Sciences, Faculty of Agriculture, Dalhousie University, Truro, NS, B2N 5E3, Canada
* To whom correspondence should be addressed

Abstract

Modern biological approaches generate volumes of multi-dimensional data, offering unprecedented opportunities to address fundamental biological questions previously beyond reach due to small or subtle effects. A fundamental question in plant biology is the extent to which below-ground activity in the root system influences above-ground traits (phenotypes) expressed in the shoot system. Grafting, an ancient agricultural practice that fuses the root system of one individual (the rootstock) with the shoot system of a second, genetically distinct individual (the scion), is a powerful experimental system to understand below-ground effects on above-ground phenotypes. Previous studies on grafted grapevines have detected rootstock influence on scion phenotypes including physiology and berry chemistry; however, the extent of the rootstock's influence on leaves, the photosynthetic engines of the vine, and how those effects changes over the course of a growing season, are still largely unknown. Here, we investigate associations between rootstock genotype and shoot system phenotypes using five multi-dimensional leaf phenotyping modalities measured in a common grafted scion: ionomics, metabolomics, transcriptomics, morphometrics, and physiology. Rootstock influence is ubiquitous but subtle across modalities with the strongest signature of rootstock observed in the leaf ionome. Moreover, we find that the extent of rootstock influence on scion phenotypes and patterns of phenotypic covariation are highly dynamic across the season. These findings substantially expand previously identified patterns to suggest that rootstock influence on scion phenotypes is complex and broad understanding necessitates volumes of multi-dimensional data previously unmet.

Background

High-throughput data acquisition has afforded unprecedented capacity to quantify and understand plant form and function. Recent advances in imaging and computation have expanded our ability to measure plant structures [1,2], and to extend those comprehensive measurements into latent space phenotypes [3]. Now broadly known as phenomics, this burgeoning field is characterized as the

acquisition and analysis of high-dimensional phenotypic data at hierarchical levels [4,5], often with an eye toward multiscale data integration. A holistic and hierarchical approach to plant phenotypic variation affords unique insights into plant evolution, and how plants change over development and in response to environmental cues and horticultural manipulation.

A fundamental question in plant biology is how root systems influence phenotypic variation in above-ground shoot systems including leaves, flowers, and fruits. Grafting, a common horticultural manipulation that joins the shoot system of one individual (the scion) with the root system of another individual (the rootstock), is commonly used in crop species to confer favorable phenotypes to commercial scions [6], including enhanced disease resistance [7,8], fruit quality, plant form [9], response to water stress [10], and growth on particular soils [11,12]. Because grafting often uses clonally propagated materials, it is possible to manipulate and replicate different combinations of root systems and shoot systems, offering a valuable experimental system in which root system impacts on shoot system phenotypes can be evaluated.

The European grapevine (*Vitis vinifera*) is among the most economically important grafted crops in the world. Grapevines are cultivated primarily for fruits used to make wine and juice, as well as for table grape and raisin production. Grafting in grapevines became widespread in the mid-1800's following the accidental introduction of the root-feeding aphid phylloxera from its native North America into Europe, where it began attacking the roots of European grapevines [13]. Because European grapevines often did not survive phylloxera infestation, most grapevine cultivation now consists of European grapevines grafted to rootstocks derived from phylloxera-resistant North American *Vitis* species including *V. berlandieri, V. riparia,* and *V, rupestris*, and their hybrid derivatives. In addition to grapevines, more than 70 major perennial crops are grafted including many fruit trees and vines [9]. In these crops, grafting decouples the breeding of shoot systems and root systems, with selection in plants targeted for use as scions focusing primarily on fruit traits, and selection in plants targeted for use as rootstocks focused on below-ground biotic and abiotic stress resistance, as well as their impacts on shoot system phenotypes.

The effects of grafting in grapevine show a remarkable breadth of scion response patterns. For example, a study of *Vitis vinifera* 'Cabernet Sauvignon' grafted to different rootstocks identified transcriptome reprogramming in the scion of grafted plants; this appeared to be a general effect of grafting to a rootstock and was not rootstock-specific [14]. In contrast, other studies have found signatures of rootstock genotype in the transcriptome in early berry development, although this distinction was lost in later development [15,16], but see [17]. Comprehensive phenomic analyses, including those that link transcriptome data with other high-throughput phenotypic assays, offer an opportunity to expand understanding of rootstock effects on grapevine shoots. In one study, leaves of the *V. vinifera* cultivar 'Gaglioppo' showed variation in stilbene and abscisic acid concentrations due to rootstock genotype, as well as differences in transcriptional profiles [18]. Likewise, gene expression, ion concentrations, and leaf shape in the cultivar 'Chambourcin' varied in response to rootstock genotype [18,19]. Collectively, these studies suggest the impacts of grafting are diverse and may vary over the course of vine development. However, to date few studies have surveyed multiple high-dimensional scion phenotypes to understand the rootstock influence on shoot system traits over the course of the growing season or the extent to which grafting effects on the scion covary with one another.

Grapevine leaves are the photosynthetic engine of the organism and a primary site for perception and response to environmental change. Leaves present a wide variety of highly variable and readily assayable phenotypes, providing an important opportunity for phenomic assessment. Grapevine leaves have been used for centuries as markers of species and cultivar delimitation, developmental variation, disease presence, and nutrient deficiency [20,21]. More recently, analysis of grapevine leaf morphology has identified genetic architecture of leaf shapes [22], developmental patterns across the season [23], and signatures of evolution in the grapevine genus [24]. Grapevine leaves respond to stress through gas and water exchange with the atmosphere [25,26] and have been shown to differentially partition the ionome depending on their position on the shoot [19] and their rootstock genotype [19,27,28]. The volume of work on grapevine leaves provides a foundation for the analysis of phenomic variation in a vineyard over a season in response to grafting.

In this study, we investigate effects of grafting on high dimensional leaf phenotypes of the hybrid cultivar 'Chambourcin' over the course of the growing season. We quantify leaf elemental (ion) concentrations, metabolite abundance, gene expression, shape, and vine physiology in a replicated rootstock trial where the hybrid grapevine cultivar 'Chambourcin' is growing ungrafted and grafted to three different rootstocks. The four root-shoot combinations ('Chambourcin' ungrafted, 'Chambourcin' grafted to three different rootstocks) are replicated 72 times in a randomized block experimental design with an irrigation treatment (Supplemental Figure 1). Data were collected either on the full 288-vine set (ion concentrations, leaf shape) or on a subset of 72 vines (the 72-vine set; metabolite abundance, gene expression, vine physiology). Using data collected at three time points that span the growing season (anthesis, veraison, and harvest), we show that ionomic, metabolomic, transcriptomic, morphometric, and physiology phenotypes reflect subtle but ubiquitous responses to grafting and rootstock genotype. Rootstock effects were often dynamic across the season, suggesting that accounting for seasonal variation could alter our understanding of grafting in viticulture.

Data Description

Leaf Ionomics

The ionome describes elemental composition of a tissue at a particular time point [29]. Three leaves per vine were collected from the 288-vine set. Leaves were sampled from a single shoot and included the youngest fully opened leaf at the shoot tip, the approximate middle leaf, and the oldest leaf at the shoot base. Whole leaves were placed in zip-lock bags in the field and stored in a cooler on ice packs, scanned for leaf shape analysis in the lab (see Leaf Shape) and then dried in coin envelopes at 50°C for one to three days for elemental analysis. Between 20 and 100 mg of leaf tissue was acid digested and 20 ions were quantified using inductively coupled plasma mass spectrometry (ICP-MS) following standard protocol [30,31] at the Donald Danforth Plant Science Center (DDPSC). Ion quantifications were corrected for internal standard concentrations, instrument drift and by initial sample mass as part of the

DDPSC Ionomics Pipeline. For each ion concentration, we computed z-score distributions and used those values as the basis for linear models. Non-standardized values were used for machine learning analysis.

Leaf Metabolomics

The metabolome comprises small molecules present in a tissue, representing a catalogue of the products of metabolic processes [32,33]. Metabolomic analysis was completed at veraison and harvest for the 72-vine set. For each vine, three mature leaves were sampled from the middle of a single shoot and immediately flash frozen in liquid nitrogen to capture the metabolic state of the leaves when attached to the vine. Leaves were sampled near midday in row and block order. Frozen leaves were transported to the University of Missouri Enology lab on dry ice and stored at -80˚C. Following the protocol of [34], whole leaves were manually ground in liquid nitrogen with a mortar and pestle, 0.5g of powder was weighed into a centrifuge tube, 1.5ml of 1:1 MeOH: ACN was added. Samples were vortexed to suspend leaf particles and sonicated for 20 minutes in an ice bath. Following extraction, samples were centrifuged for 10 minutes at 3,000 g and filtered with a 0.22 PTFE syringe filter into a 1.5ml sample vial before injecting into a Waters XEVOTM QToF LCMS system (Waters Corporation, Milford, MA, USA). Chromatographic separation was achieved using a Waters Acquity TM Ultra Performance LC H-Class system (Waters Corporation, Milford, MA, USA) equipped with Waters Acquity BEH C18 column (2.1mmx150mm and 1.7um particle size) and a diode array detector. Samples were injected in random order across the sampling periods. The injection volume was set at 2.5ul and the flow rate was set at 0.4 ml/min. The mobile phase consisted of 0.1% formic acid in water (solvent A) and 0.1% formic acid and 5% water in acetaldehyde (solvent B) and the gradient was as follows: 100% A for 0.5 min; 0.5-18min increased to 99% B; 18-19 min. held at 99% B; mobile phase was re-equilibrated for 2 min between runs. Diode array was monitored at 225-500nm. Mass spectrometry was performed on a XevoTM QTof (Waters Corporation, Milford, MA, USA). The electrospray ionization (ESI) was operated in both positive or negative ionization modes in separate runs. The scan range was set as m/z 50-1500 with 0.2

sec accumulation time. MS settings were as follows: capillary voltage was 2.5kV; cone voltage ramped from 20-40V; collision energy was set to 6V; detector voltage was set to 1950V; desolvation gas was set to 1000 L/hour; cone gas was set to 50 L/hr; source temperature was 120℃ and desolvation temperature was set at 550℃.

LC-MS instrument files were converted to .cdf format and uploaded to XCMS online [35] for chromatogram normalization and feature detection via "single job" parameters. Identified metabolomic features were used as the basis of a principal components (PC) analysis. The top 20 PCs were treated as distinct phenotypes to model according to the experimental design. In PCs that varied significantly by rootstock, features that loaded more than 1.96 standard deviations above or below the mean were fit independently with the same model design.

Leaf Gene Expression

The youngest fully-opened leaves on two shoots were collected from each plant of the 72-vine set (see Study Design). The two leaves, which were distinct from leaves used for ionomics, leaf shape, metabolomics and physiology data collection, were pooled for RNA sequencing. Samples were sequenced using 3'-RNAseq, a method ideal for organisms with reasonably characterized reference genomes [36]. The first 12 nucleotides from each read were trimmed to remove low-quality sequences using Trimmomatic (options: HEADCROP:12; [37]). Low quality trimmed reads were additionally identified based on overrepresentation of kmers and removed using BBduk (April 2019 release) [38]. Trimmed and QC-controlled reads were mapped to the 12Xv2 reference *Vitis vinifera* genome [39,40] using STAR (v2.7.2b) [41] with default alignment parameters. RNAseq read alignments were quantified using HTSeq-count (v0.11.2) [42] and a modified version of the VCost.v3 reference *V. vinifera* genome annotation [40]. To capture mis-annotated gene body boundaries in the genome, all gene boundaries in the annotation were extended 500 bp.

Variation in gene expression was assessed using two methodologies. First, we identified individual genes which responded to specific factors in the experimental design using DESeq2 (v1.24.0)

[43]. Each gene was fit with the model "~ Block + Irrigation + Phenology_Rootstock" where the 'Phenology_Rootstock' model term was used to understand the potential interaction of phenology and rootstock. Differentially expressed genes were identified for each pairwise contrast in the model. Genes were filtered to a gene set that included only genes with a normalized count greater than or equal to two in at least five samples. Second, we used principal component analysis (PCA) to collapse variation in co-expressed genes into fewer dimensions. Normalized count-filtered genes from DESeq2 were transformed using the variance stabilizing transformation (VST; [44]) and input into a PCA. We then analyzed the top 100 PCs in the context of the broader experimental design. We previously showed that the transcriptome varied by the time of collection and was potentially interacting with the rootstock effect [19]. Moreover, the other modalities in this study point to weak if any effects from the irrigation treatment. Due to the nature of the vineyard design, we could not identify both irrigation and time effects (marked by row) in a single model (irrigation and row are collinear; see Study Design). To approximate the impact from time of collection (row) in the vineyard on gene expression, linear models were first fit to remove variation imparted by irrigation from each of the top 100 PCs. The residuals were then used as the basis for linear models and machine learning analysis.

Leaf Shape

All leaves from a single shoot directly emerging from a trained cordon were collected from each vine in the 288 vine set at 80% anthesis and veraison. At harvest, we collected only the oldest (first emerging leaf), middle (estimated from the middle of a whole shoot), and youngest (smallest fully emerged leaf at the shoot tip, >1cm). Leaves were collected approximately in row order (from south to north) and stored in a cooler. Each leaf was imaged using an Epson DS-50000 scanner. Following scanning of leaves for leaf shape analysis, the oldest, middle, and youngest leaves were dried and used to estimate leaf elemental composition (see Ionomics). While all leaves were collected from a single shoot, only the oldest, middle, and youngest were used in this analysis.

We assessed leaf shape using generalized procrustes analysis (GPA) of landmarks. For the three leaves per vine used in leaf shape analysis, 17 homologous landmark features were identified [22]. The GPA-rotated coordinate space was used for all subsequent statistical analysis including PCA in order to summarize variation in leaf shape [45]. From the PCA, we extracted the top 20 PCs and fit linear models and machine learning models to describe variation.

Vine physiology

Intracellular CO_2 concentration, stomatal conductance and leaf transpiration rate were measured at midday (10am to 1pm) on one fully expanded sun-exposed leaf for each of the vines in the 72-vine set. Measurements were taken using an LI-6400XT Portable Photosynthesis system coupled with a pulse amplitude-modulated (PAM) leaf chamber fluorometer (Li-Cor, Inc., Lincoln, NE, USA) with the following parameters: incident photosynthetic photo flux density level of 1000 μmol m−2 s−1 generated by a red LED array and 10% blue light to maximize stomatal opening, CO_2 mixer of 400 umol/s, fixed flow of 300 umol/s, and ambient leaf and block temperature. Soil moisture was measured for each plant in the 72-vine set using a fieldScout TDR 300 Moisture meter equipped with 20 cm rods (Spectrum Technologies, Inc. Aurora, IL, USA). Midday stem water potential was measured using a pressure bomb/chamber (PMS Instrument Co., Albany, OR, USA) after enclosing the leaves in an aluminum foil bag for at least 15 minutes to equilibrate the water potential of the xylem in the stem to that attached leaf.

Analyses

Leaf ionome

To characterize the leaf ionome over the growing season, we sampled the youngest, middle, and oldest leaf from a single shoot from each of the vines within the 288-vine set at three phenological stages (Figure 1). Bivariate correlations showed that ion concentrations are not independent of each other, but the strength and direction of relationships between ions vary with respect to phenological stage and leaf

position (Supplemental Figure 2). As such, we fit independent linear models to each ion. Leaf position, phenological stage, or the interaction of phenological stage and leaf position explained the highest amount of variation for most ions (Figure 1A-B). Many ions significant for the interaction showed a clear signal of leaf position at anthesis and veraison, and either no explainable variation or muted variation at harvest. For example, calcium (Figure 1B) varied with leaf position (22.7%; $p < 1e-05$), phenology (24.0%; $p < 1e-05$), and their interaction (7.4%, $p < 1e-05$). All possible pairwise combinations of leaf position were significantly different at anthesis, and both the youngest and middle leaves were different from the oldest leaves at veraison and harvest. In the case of potassium (Figure 1B), significant variation was explained by leaf position (16.1%; $p < 1e-05$), phenology (19.6%; $p < 1e-05$), and their interaction (10.6%; $p < 1e-05$). However, post-hoc comparisons showed that differences were present only at anthesis and veraison.

The rootstock showed remarkable influence on the composition of the leaf ionome. All ions except aluminum, sodium, and zinc were significant for rootstock as a single fixed effect (Figure 1A). Rootstock explained between 0.4% (rubidium; $p = 3.2e-05$) and 14.3% (nickel; $p < 1e-05$) of variation in each ion (Figure 1A). Ions that responded weakly to the interaction of leaf position and phenology tended to show significant variation explained by the interaction of rootstock and phenology. These ions showed similar patterns to the leaf position by phenology interaction where clear signal was exhibited at anthesis and veraison then is either absent or muted at harvest. For example, cobalt was most abundant in ‘1103P’-grafted vines at anthesis (Figure 1C). At veraison, both ‘1103P’-grafted and ‘SO4’-grafted had elevated concentrations compared to Ungrafted and ‘3309’-grafted vines. However, by harvest, cobalt concentration variation was muted and only ‘SO4’-grafted vines showed evidence of elevated concentration. Similarly, nickel showed significant variation partitioned into the rootstock by phenology effect (Figure 1C). Both anthesis and veraison show reduced nickel concentration in ‘1103P’-grafted vines and elevated concentrations in ‘SO4’-grafted vines. However, at harvest, no comparisons are significant.

Machine learning on ion concentrations confirms that the leaf ionome contains a signature from the rootstock genotype and the interactions of rootstock genotype with phenology and leaf position. A

random forest model trained to predict rootstock showed an overall accuracy of 75.2% (Figure 1D). Ions important for this classification were nickel (MDA=0.089), molybdenum (MDA=0.058), and magnesium (MDA=0.054), corroborating the rootstock term's significance in the linear models. Notably, when we trained a model to simultaneously predict rootstock and phenological stage, rootstock prediction accuracy increased appreciably (Figure 1E). For example, the ability of the model to detect ungrafted vines (the balanced accuracy of ungrafted predictions) improved from 81.7% accuracy overall to 91.1% accuracy at anthesis and 85.9% at harvest. Generally, performance at veraison matched the rootstock-only model performance. The ions most important for this joint (rootstock/phenological stage) prediction were nickel (MDA=0.167), phosphorus (MDA=0.110), and strontium (MDA=0.065). The rootstock by phenology model term was significant in the linear models for these ions, but was not a largest descriptor of variation. The joint prediction of rootstock and leaf position performed substantially better than chance ($p < 1e-05$), but accounting for leaf position did not improve rootstock prediction as was the case in the joint prediction of rootstock and phenology (Figure 1F). Ions important for this classification were sulfur (MDA = 0.051), rubidium (MDA = 0.051), and nickel (MDA = 0.049).

Leaf metabolomics

We performed untargeted metabolomics on leaves from the 72-vine set at veraison and harvest, quantifying the concentrations of 661 metabolites (Figure 2). The top 20 PCs accounted for a total of 67.3% of the total metabolomic variation, with the top three capturing 23.1%, 9.2%, and 6.2%, respectively. Individual PCs after the top 20 explained less than 0.82% of the metabolome. Linear models for each of the top 20 PCs found that the strongest drivers of variation in leaf metabolomics were phenology and temporal blocking factor. For example, 90.6% of variation on PC1 was due to phenology ($p < 1e-05$; Figure 2A). PC2 primarily reflected the interaction of phenology and temporal block (26.4%, $p < 1e-05$) and temporal block as a main effect (18.9%, $p < 1e-05$). The patterns of variation attributable to PC2 were similar in PCs 3-10 (Figure 2A).

PC17 was controlled by rootstock as a main effect (18.5%, $p < 1e-03$; Figure 2B). On PC17, ungrafted vines were significantly different from vines grafted to '3309C' ($p = 0.02$) and 'SO4' ($p < 1e-05$). Vines grafted to '1103P' were also significantly different from vines grafted to 'SO4' ($p = 0.009$). Metabolites that loaded more than 1.96 sd from the mean loading on PC17 were extracted and independently fit to additional linear models. We identified four metabolite features (M374T1 [rt = 1.33, m/z = 374.1146], M117T1 [rt = 0.61, m/z = 117.0583], M175T1_1 [rt = 0.87, m/z = 175.1269], and M333T1_3 [rt = 0.71; m/z = 333.1582]) which were influenced by rootstock as a main effect and the metabolite (M112T1 [rt = 1.48, m/z = 112.0061]) which was influenced by the interaction of rootstock genotype and phenological stage. At this time, the identification of these features remains unknown.

Linear discriminant analysis confirmed that many experimental factors likely influence the metabolome. For example, when trained to maximize variation between classes of rootstocks, the model identified a space that weakly separates '1103P'-grafted and 'SO4'-grafted vines from Ungrafted and '3309C'-grafted vines (LD1) and separates '3309C'-grafted vines from other classes (on LD2) (Figure 2C). Despite this, machine learning showed minimal predictability for any class other than phenology, which was predictable with an accuracy of 100% for withheld samples. Rootstock genotype based on the metabolome was not predictable with accuracy only marginally better than chance (34.6%).

Gene Expression

We performed 3'-RNAseq on the 72 vine set at three time points (Figure 3). We identified variation in 23,460 genes that had a DESeq2-normalized count greater than two in at least five samples. Using a traditional analysis framework, all genes returned as significantly differentially expressed by rootstock appeared to be false positives, evidenced by a single extreme outlier altering group means. Hierarchical clustering of the 500 most variable genes after variance stabilizing transformation (VST) showed strong latent structure in the transcriptome and that most variation in the transcriptome was explained by phenological stage (Figure 3A). The top 100 PCs on the VST-transformed gene counts accounted for nearly 92.3% of variation in the transcriptome. Linear models on each of the top 100 PCs

indicated that 82.4% and 61.4% of the variation on PC1 and PC2 respectively were attributable to the phenological stage (Figure 3B-C). Row was also a significant descriptor of variation as a single, fixed effect and in interactions with rootstock and phenological stage. For example, row accounted for 36.0% and 43.3% of the variation on PC4 and PC6, respectively. Interacting with phenological stage, row accounted for >10% of variation on 17 additional PCs.

Patterns of gene expression identified through LDA corresponded to phenological stage, vine row, and rootstock. LDA separated phenological stages into three distinct, non-overlapping groups in the space spanning LD1 and LD2 (Supplemental Figure 3). When trying to separate rows into distinct classes, the model converged on a 'horseshoe' shape in the LD1- LD2 space (Figure 3D). LD1 maximized the variation between row 8 (sampled early in the day) and row 16 (sampled a few hours later). LD2 maximized the separation of both rows 8 and 16 with row 12 (the row sampled in the middle of the sampling window). A model trained to separate rootstock classes (Figure 3E) showed that LD1 separated the rootstock 1103P from other rootstock genotypes, and LD2 primarily separated the rootstock '3309C' from ungrafted vines (Supplemental Figure 3).

Formal machine learning on gene expression PCs largely supported the linear models. A random forest trained to predict phenological stage classified testing samples with 92.9% accuracy. Anthesis was the most predictable class with a balanced accuracy of 100%; veraison and harvest displayed balanced accuracies of 92.7% and 92.4%, respectively. The PCs most important in phenology prediction were PC1 (MDA = 0.16) and PC2 (MDA = 0.12). Gene expression PCs were unable to predict rootstock, with a total prediction accuracy of 23.4%. While no features were especially important in the prediction processes, PC44 showed the largest mean decrease in Gini impurity corroborating its signal in the linear models.

Leaf shape

We collected leaves from the 288-vine set at three time points and landmarked a total of 2,422 leaves (Figure 4). Homologous leaf landmarks were used for generalized procrustes analysis (GPA). PCA

on the GPA-rotated coordinates revealed ~97.2% of the total shape variation was captured by the top 20 principal components with PC1, PC2, and PC3 explaining 24.1%, 19.0%, and 13.3% of the variation respectively. Lower values on PC1 primarily capture leaves with shallow petiolar sinuses and short midvein distance from the depth of the superior sinus to the top of the midvein, whereas higher values on PC1 capture the opposite (Figure 4A). Similarly, lower values on PC2 capture deep petiolar sinuses combined with very shallow superior sinuses, and vice versa for higher values. PC3 primarily captures asymmetry (Figure 4A).

In total, only 5.76% of variation on PC1 was explained by the experimental design, with most variation explained by phenology (2.63%; padj < 1e-05), rootstock (0.95%; padj < 0.001), leaf position (2.61%; padj = 0.03), and the interaction of phenology and leaf position (0.62%; padj = 0.009) (Supplemental Figure 4A). Post-hoc mean comparisons on PC1 showed that shapes of leaves from ungrafted vines were significantly different from leaves of vines grafted to 1103P ($p < 0.001$), 3309C ($p < 0.001$) and SO4 ($p < 0.001$) (Supplemental Figure 4B). Moreover, PC1 captured subtle variation in the leaf position by phenological stage interaction where middle leaves showed significant differences between anthesis and veraison ($p < 1e-03$), and the oldest leaves showed significant differences when comparing anthesis to veraison ($p < 1e-05$) and anthesis to harvest ($p < 1e-03$).

For PC2, 61.4% of variation could be assigned to an experimental factor. This included significant variation from leaf position (46.9%, padj < 1e-05), phenology (1.4%; padj < 1e-05), and the interaction of leaf position and phenology (12.05%; padj < 1e-05; Figure 4D). Specifically, younger leaves tended to have shallower sinuses and exaggerated superior sinus depths (higher values on PC2), whereas older leaves tended to develop deeper petiolar sinuses and more shallow superior sinuses (lower values on PC2). The degree of this separation decreased across the season, and the shapes converged on the mean leaf shape on PC2, consistent with the middle leaf at all three phenological stages. PC2 additionally reflected the interaction of leaf position and rootstock (0.22%; $p = 0.04$; Supplemental Figure 4B), but post-hoc comparisons did not find any significant pairwise comparisons.

Machine learning on the GPA-rotated coordinate space identified moderate division of developmental and phenological classes. Random forest models could predict the leaf position with 73.1% accuracy, with the most important feature being the y-component of the leaf apex (MDA = 0.051). A model trained to predict phenology performed at 64.3% with the most important features being the x-components of the points corresponding to superior sinus depth (left sinus MDA = 0.030, right sinus MDA = 0.019). A model trained to predict rootstock performed only marginally better than chance at 28.1% accuracy.

Vine physiology

For the 72-vine set, we measured intracellular CO_2 concentration (C_i), stomatal conductance (g_s), leaf transpiration, water potential (ψ), and soil moisture (Figure 5). Each physiological trait varied significantly across phenology and the block by phenology interaction (Figure 5A). For example, at harvest, we observed specific differences in leaf CO_2 concentration (A vs C: p=0.003; B vs C: p=0.002) and leaf transpiration (A vs B: p < 1e-03; A vs C: p < 1e-05; B vs C: p < 1e-05). Leaf transpiration and stomatal conductance varied significantly with the interaction of rootstock and phenology. A post-hoc comparison of means showed that leaf transpiration and stomatal conductances were elevated in 'Chambourcin' vines grafted to '1103P' at veraison as compared to leaves of ungrafted vines (leaf transpiration: p = 0.001; stomatal conductance: p = 0.002 Figure 5B-C).

Phenomic trait covariation

Four leaf data modalities consisted of at least 10 traits and were measured for all plants in the 72-vine set (leaf ionome, leaf metabolomics, gene expression, leaf shape). Using these data, we explored the extent to which different phenotypes covaried over phenology and rootstock genotype (Figure 6; Supplemental Figure 5; Supplemental Figure 6). Within each phenotyping modality, we summarized the primary dimensions of variation using PCA (see Methods). From each PCA, we extracted the top 10 PCs,

which explained a total of 88.9% of variation in the ionomics PCA (iPCA), 55.9% of the variation for the metabolomics PCA (mPCA), 74.8% of the variation in the gene expression PCA (gPCA) and 87.9% of the variation in the leaf shape PCA (sPCA).

Pairwise correlations of each PC within each phenological stage showed diverse correlation magnitudes and directions both within a phenotyping modality and between phenotyping modalities (Figure 6A-C; Supplemental Figure 5). Generally, the strongest relationships were between PCs within phenotypic modalities. For example, the strongest correlations identified were between gPC1 and gPC2 at anthesis (r = 0.85, CI = [0.81, 0.87]; Supplemental Figure 5A, and mPC1 and mPC2 at harvest (r = -0.78, CI = [-0.82. -0.76]). Correlations between modalities represented a diversity of responses across phenological stages. For example, the correlation between gPC4 and sPC3 is similar across the phenological stages, but only the correlation at veraison is significant (r = 0.41, CI = [0.34, 0.47]; Supplemental Figure 5B). Correlations such as between mPC3 and gPC6 were similar and significant at both veraison (r = -0.44, CI = [-0.50, -0.37]; Supplemental Figure 5C) and harvest (r = -0.37, CI = [-0.45, -0.28]; Supplemental Figure 5C). While many correlations varied over the course of the season, some relationships entirely shifted in direction. For example, the correlation between mPC3 and mPC6 shifted from a positive significant relationship (r = 0.58, CI = [0.52, 0.63]) at veraison to a negative significant relationship at veraison (r = -0.66, CI = [-0.73, -0.59]) (Supplemental Figure 5D).

Pairwise comparisons of PCs within each rootstock genotype show a suite of traits with significant presence/absence variation in significant correlations. Where each phenological stage showed modularity by phenotyping modality, variation over rootstock genotype shows a strong ionomics module with latent combination of other modalities interspersed (Supplemental Figure 6). For example, in ungrafted vines, mPC1 was correlated with four PCs from the ionome (Supplemental Figure 6A). Each of the other rootstock genotypes have dramatically different topologies with the ionome tending to be more connected within the ionome and connected to other modalities only on the periphery (Supplemental Figure 6B-D). Examples of presence/absence variation are shown in small modules of two latent phenotypes that are present in only one rootstock genotype. For example, in the ungrafted vines, the

correlation between gPC4 and mPC3 was significant (r = -0.58, CI = [-0.65, -0.51]) and, in '1103P'-grafted vines, the correlation between mPC3 and sPC6 (r = 0.59, CI = [0.53, 0.70]) was significant.

Discussion

In this study, we used grafted grapevines as an experimental system for characterizing root system impacts on high dimensional leaf phenotypes over the course of a growing season. We detected ubiquitous but subtle effects of the root system on all assayed phenotypes, and demonstrated that rootock influences on leaf phenotypes can be season-specific. The strongest signals of rootstock influences on leaves were observed in the ionomics dataset, phenotypes for which the root systems have a noted and well-understood role.

Phenology explains significant variation in all leaf phenotypes

The timing of sampling or phenological stage of the vines (anthesis, veraison, harvest) was the strongest driver of phenotypic variation for most leaf phenotypes. For example, all 20 ions varied with phenology and most ions showed that phenology, or the interaction of phenology with leaf developmental position, was the strongest source of variation (Figure 1). Nearly one third of all measured transcripts responded to seasonal variation, and the strongest effects on the transcriptome were phenology and row, a correlate for the time within a three-hour sampling window. The only phenotype for which phenology was not the most explanatory factor is leaf shape. Consistent with previous studies [23], we confirm that most of the leaf shape variation measured reflects development along a single shoot, but much of this variation is explained via interaction with phenology. These data highlight the dynamic nature of biological processes taking place within grapevines over the course of a season.

The seasonal component to grapevine phenotypic variation is a subject of much research, especially in the berry. In studies designed to quantify molecular underpinnings of terroir, seasonal variation was identified as the strongest signal in the metabolome [46–49]. Several studies have

characterized transcriptomic variation over the course of the season. For example, in conjunction with metabolomics, seasonal variation of berry development was used to identify transcriptomic and metabolomic developmental markers in 'Corvina' [50]. Follow-up analysis showed that nearly 18% of transcripts varied seasonally [51]. Grapevine leaves also vary tremendously in shape over the growing season [23] and are stable over multiple growing seasons; interestingly, grapevine leaves are patterned in the previous year, and the climate of the season in which the leaves were patterned influence aspects of leaf shape [52,53].

Grafting and rootstock genotype exhibit a complex and subtle signal on leaf phenotypes

Consistent with previous studies, we confirm that grafting, as well as rootstock genotype, has a complex effect on phenotypic variation in the scion (the grafted shoot system). Most notably, we show that the rootstock to which a scion is grafted influences ion concentrations in leaves. Rootstock genotype is predictable from ion concentrations in the leaves; further, this signal is strengthened when phenological stage is included in the model. For example, we previously showed that nickel concentration was elevated in vines grafted to the rootstock 'SO4' [19]. At a similar point in the season, we observe the same pattern, but by harvest, nickel was almost entirely excluded from the leaf. This suggests that the biological implications of this differential uptake could be missed if not surveyed across the season. We also confirm that rootstock genotype influences the metabolome of grafted grapevine, in some cases in a season-specific manner. In the transcriptome, PCA was able to identify dimensions of variation that were significantly described by rootstock and the interaction of rootstock and time of day, confirming prior observations [19]. Patterns of gene expression were associated with rootstock in some analyses; for example, supervised methodologies identified linear discriminants in the PC space that separated some rootstock genotypes. However, gene-by-gene analysis found no genes modulated by rootstock genotype, or even just from the act of grafting that were not driven entirely by a single outlier. We suspect these results are due, at least in part, to the strength of the phenology effect overpowering more subtle variation imparted by rootstock genotype. Finally, of the physiology traits we measured, leaf transpiration and

stomatal conductance were higher vines grafted to ‘1103P’ in the middle of the season. Thus, the impact of grafting on leaf phenotypic variation varies by phenotype. Regardless, we identify subtle but ubiquitous effects from rootstock genotype on shoot system phenotype.

Understanding of rootstock genotype influence shoot system phenotypes is a growing area of research, especially in grapevine. For example, in ‘Cabernet Sauvignon’, grafting increased ion uptake globally and some rootstock genotypes provide a clear signal in the scion [28,54]. Also, the metabolome is a key driver of the formation of the graft junction and some key metabolites could be responsible for graft incompatibility [55]. Building on this work, targeted metabolomics showed two classes of metabolites, flavanols and stilbenes, were differentially abundant at graft junctions and in the rootstocks of ‘Cabernet Sauvignon’ vines one month after grafting [56]. However, flavanols were not differentially abundant in the scion, but scion stilbene concentrations were apparently controlled by rootstock genotype. The effect of rootstock genotype on the scion transcriptome is perhaps the most varied. For example, ‘Cabernet Sauvignon’ shoot apical meristems show no effects by rootstock genotype [14], but berries of the same cultivar do, although the effect is tempered by seasonal variation [15]. Variation in ‘Chambourcin’ leaf shape is also driven by rootstock genotype, especially in conjunction with differences in irrigation [19]. Collectively, these studies all suggest that rootstock genotype influences scion phenotypes, but those effects will vary by phenotype, scion genotype, and perhaps other experimental conditions. Data presented here confirm and expand upon previous observations of rootstock effects on scion phenotypes. Notably, the robust experimental design (288 vine set and 72 vine set comprising replicates of three rootstocks grafted with a common scion and an ungrafted control), coordinated collection of five multi-dimensional leaf phenotypes, and inclusion of three sampling points spanning the growing season allow us to hone in on the comprehensive nature of rootstock influences on the scion. Further, this thorough analysis demonstrates that rootstock effects on scion phenotypes shift in magnitude over the course of the season, indicating that aspects of time are tremendously influential to the observed results regardless of phenotype.

Phenomic covariation warrants work toward latent phenotypes

In the present study, we assess the extent of covariation among leaf phenotypes. For the primary dimensions of variation in each data type, within-data-type correlations are strongest when accounting for phenological timing. Correlations also exist between phenotypes, suggesting room for the analysis of latent phenotypic structure for experimental questions. For example, aspects of the metabolome were frequently correlated with the transcriptome and leaf shape when accounting for both phenological stage and rootstock genotype. Interestingly, correlations within and between data types are highly dynamic over a growing season and across rootstock genotype. For example, several correlations with leaf shape were present at veraison, but were not detected at anthesis and harvest. Moreover, the topology of connections in the ionomic network was variable over the rootstock genotype (Supplemental Figure 6). This variation in topology confirms that root system genotype has a strong influence on shoot system elemental composition, and suggests that root system genotype can alter correlative patterns in the ionome. We believe the work of understanding phenomic covariation warrants further investigation, specifically, by further including additional phenotypes such as lncRNA expression [57,58], epigenetics [59], and microbiomes [60,61]. Much of the work constituting phenomics in grapevine has addressed how berries develop over the growing season, how cultivars differ from one another, and how the concept of terroir influences wine [46,47,50,62–64]. Despite data integration techniques becoming more popular, there are still many open questions as to what analytical methods are most appropriate and how to most effectively utilize them (reviewed for grapevine in [65,66]; reviewed broadly in [67,68]). Ongoing work attempts to integrate high-dimensional phenotypic datasets generated within a single organ system (e.g., leaves); and future studies will expand this to explore phenomic covariation in and among organs, over time, and across space.

Potential Implications

Our work on the influence of root system genotype on shoot system phenotype has broad implications for a holistic understanding of how plants detect and respond to changing environmental

conditions. In particular, this study highlights the influence of root system genotype and its interaction with phenology on shoot system phenotype: there is a seasonal component to the extent to which rootstock shapes phenotypic variation in the scion. Expanding this multi-dimensional understanding of phenotypic variation over time to include different tissues (e.g., root architecture, floral and fruit development), and different spatial scales (replicated root-shoot combinations located in geographically distinct vineyards) presents a challenging but exciting next frontier. Of particular note, patterns of phenomic covariation derived from complex datasets have implications for understanding how individuals perceive and respond to their environments, and how that response is coordinated throughout the plant body. This work is relevant for breeding efforts aimed at optimizing yield and other desired traits that can be optimized, or constrained by, phenotypic variation elsewhere in the plant.

Methods

Study Design

Data were collected in 2017 in an experimental rootstock trial at the University of Missouri's Southwest Research Center near Mount Vernon, MO (37.074167 N; 93.879167 W; Supplemental Figure 1). The rootstock trial includes the interspecific hybrid cultivar 'Chambourcin' growing ungrafted (own-rooted) and grafted to three rootstocks: '1103P', '3309C', and 'SO4' (Supplemental Figure 1D). Each of the four rootstock-scion combinations was replicated 72 times for a total of 288 vines planted in nine rows. Each row was treated with one of three irrigation treatments: full evapotranspiration replacement, partial (50%) evapotranspiration replacement (reduced deficit irrigation; RDI), or no evapotranspiration replacement (Supplemental Figure 1A). However, rainfall in 2017 likely mitigated the applied irrigation treatment (see Supplemental Note at: https://github.com/PGRP1546869/mt_vernon_2017_leaf/blob/main/On_the_irrigation_treatment.pdf). Vine position in the vineyard corresponded to time of sampling for some phenotypes, as samples were taken from one end of the vineyard to the other over the course of two to three hours. Because vineyard

microclimates and sampling time may be associated with phenotypic variation, we defined ‘temporal block’ as a factor that captures this spatial and temporal variation inherent in sampling. Unique rootstock-scion combinations were planted in cells of four adjacent replicated vines (Supplemental Figure 1B), with rows consisting of eight cells (32 vines/row). To our knowledge, a field-planted rootstock experimental vineyard of this size and age is rare. For some phenotypes (leaves for ionome and leaf shape analysis), it was possible to collect samples from all vines in the experimental vineyard (the 288-vine set; Supplemental Figure 1C). For other phenotypes (physiology, metabolomics, and gene expression), time and/or expense associated with the phenotyping process required that we reduce sampling to a nested set of 72 vines representing the middle two vines in each four-vine cell (the 72-vine set; Supplemental Figure 1C). All phenotypes were assayed \at three phenological stages: anthesis (~80% of open flowers; 22 May 2017); veraison (~50% of berries had transitioned from green to red; 30 July 2017); and immediately prior to harvest (25 September 2017).

Linear Models

Linear models were fit to the 20 measured ion concentrations, the top 20 PCs of the leaf metabolome, the top 100 PCs of the leaf transcriptome, the top 20 PCs of leaf morphospace, and each measured physiological trait. Outliers were detected using the R function ‘anomalize’ (options: alpha=0.03, max_anoms=0.1). Each model was fit with fixed effect factors representing phenological stage (anthesis, veraison, or harvest), rootstock (Ungrafted, ‘1103P’, ‘3309C’, or ‘SO4’), leaf position (youngest, middle, or oldest; only used in leaf morphology and leaf ion concentration models), and all pairwise interactions of those terms. Both irrigation and block were included as fixed, non-interacting effects with the exceptions of physiology and metabolomics, for which we allowed the interaction of ‘Block’ as it correlates with the time of sampling, potentially capturing temporal variation. Row, an additional correlate for time and spatial variation, was included in place of a temporal block for the gene expression models after removal of the variation attributable to irrigation, a factor collinear with row. All linear models were interpreted using a type-3 sum of squares computation using the R package ‘car’ [69].

Estimated p-values for each term in the models were corrected for multiple tests (within phenotype) using FDR correction as implemented by the R package 'stats' [70]. Results from the models are reported as the variation explained by a particular term in the model and the estimated p-value. When appropriate, post-hoc mean comparisons were computed using the package 'emmeans' [71]. Where multiple linear models were being simultaneously interpreted, we applied a Bonferonni correction to reduce the number of false positives.

Machine Learning to Identify Rootstock Effects

For visualization of between-class variation, we fit linear discriminant analysis models (LDA) to the full phenotypic data sets of ionomics, metabolomics, gene expression, and leaf morphology using the 'lda' function of the R package 'MASS' [72]. Projections of all samples into the LD space were plotted using ggplot2 [73]. In addition, we employed machine learning to capture subtle experimental effects. We partitioned phenotypic data sets into 80% training partitions and 20% testing partitions. Models were fit to predict the phenological stage from which a sample was taken, the rootstock to which the scion was grafted, and the joint prediction of phenology and rootstock. We also tested the predictability of leaf position for ionomics and leaf shape, and the interaction of rootstock and leaf position for ionomics. We used the 'randomForest' [74] implementation of the random forest algorithm. Models were fit and tuned using the R package 'caret' [75]. Each performance was assessed using accuracy, with performance on each class being assessed using the balanced accuracy, the midpoint of class-wise sensitivity and specificity. Where appropriate, models were compared to 'chance', or the occurrence frequency of each class. Confusion matrices were visualized from the out-of-bag predictions using ggplot2. Important features were identified from the randomForest object based on a phenotype-specific mean decrease in model accuracy (MDA).

Phenomic trait covariation

We extracted ionomics, metabolomics, gene expression, and leaf shape data for the youngest available leaf from the 72 vine-set. Each class of phenotypic data was summarized along the primary dimensions of variation using PCA. For each class, we extracted the top 10 PCs and fit Pearson's correlations across all pairs of PCs at each phenological stage. P-values from computed correlations were corrected using the FDR method from the package 'stats' [76]. Correlations and their strengths were visualized using the R package 'igraph' [77]. Example correlations were reported after running 10,000 bootstrapped subsamples of 90% of data for paired traits. From the distribution of estimated correlation coefficients, confidence intervals were computed from the 0.025 and 0.975 quantiles. A subset of example correlations were plotted using the R package 'ggplot2' [73].

Acknowledgments:

This work was funded by the National Science Foundation Plant Genome Research Project 1546869. We thank members of the Miller Lab at Saint Louis University and the Donald Danforth Plant Science Center, members of the Kovacs Lab at Missouri State University, members of the Kwasniewski Lab at the University of Missouri, and members Londo Lab at the USDA-ARS Grape Research Unit for vineyard sampling and sample processing. We express special thanks to Matthew Rubin and Elizabeth Kellogg at the Donald Danforth Plant Science Center for valuable comments on the manuscript.

Figure Legends:

Figure 1: The ionome shows strong signal from rootstock genotype, leaf position, and phenological stage **(A)** Percent variation captured in linear models fit to each of 20 ions measured in the ionomics pipeline. Presence of a cell indicates the model term (top) was significant (FDR; p.adj < 0.05) for that ion (left). **(B)** Example ions shown to vary significantly by the interaction of leaf position and phenological stage. Boxes are bound by 25th and 75th percentile with whiskers extending 1.5 IQR from the box. (**C**) Example ions shown to vary significantly by the interaction of rootstock genotype and phenological state. Boxes

are bound by 25th and 75th percentile with whiskers extending 1.5 IQR from the box. (**D**) Standardized heatmap for out-of-bag (OOB) predictions by a random forest trained to predict rootstock genotype, **(E)** the interaction between rootstock genotype by phenology, and **(F)** the interaction between rootstock genotype and leaf position.

Figure 2: The metabolome is influenced by rootstock genotype, phenological stage, and time of sampling. **(A)** Percent variation captured in linear models fit to each of the top 20 principal components of the metabolome (661 measured metabolites). Presence of a cell indicates the model term (top) was significant for that PC (left, percent variation explained by the PC in parentheses). **(B)** The distribution of projections onto PC17, the strongest captured rootstock effect in the metabolome. Boxes are bound by the 25th and 75th percentiles with whiskers extending 1.5 IQR from the box. **(C)** Projections of all samples into the first two dimensions of a linear discriminant space trained to maximize variation between rootstock genotypes.

Figure 3: Gene expression primarily responds to time of season and circadian correlates
(A) Heatmap showing 500 genes with the highest variance following the filtering of lowly expressed genes and gene-by-gene variance stabilizing transformations (VST) ordered by example model factors (below). **(B)** Percent variation captured in linear models fit to the top 100 Principal Components of the VST-transformed gene-expression space. Presence of a cell indicates the model term (top) was significant for that PC (left, percent variation explained by the PC in parentheses). **(C)** Projections of all samples into the first two principal component dimensions to show that the largest descriptors of variation are due to phenology. **(D)** Projections of all samples into the first two dimensions of the linear discriminant space trained to maximize variation between the rows of the vineyard, and **(E)** rootstock genotype.

Figure 4: Leaf shape variation is primarily determined by shoot position but changes over the season

(A) Representative shapes showing leaf variation (-3 sd, mean, +3 sd) captured in each of the top 4 principal components of the Generalized Procrustes Analysis-rotated leaf shapes. **(B)** Projections of all leaves into the first two dimensions of principal component space colored by the strongest determinant of variation in the top two PCs. **(C)** Projections of all leaves into the first two dimensions of a linear discriminant space trained to maximize variation between phenological stages. **(D)** Variation in leaf shape captured on PC2 shown by leaf position and phenological stage. Large points represent the mean of the group when projected onto PC2. Bars surrounding the mean show one standard deviation. Variation in each group is shown as a composite leaf trace scaled to a standard size and centered over the mean.

Figure 5: Vine physiology measurements show signal from most experimental manipulation

(A) Percent variation explained by model terms (top) from linear models fit to each of four physiology traits (left). **(B)** Variation in leaf transpiration rate for each rootstock genotype over the course of the season. Boxes are bound by the 25th and 75th percentiles with whiskers extending 1.5 IQR from the box. **(C)** Variation in stomatal conductance for each rootstock genotype over the course of the season. Boxes are bound by the 25th and 75th percentiles with whiskers extending 1.5 IQR from the box.

Figure 6: Trait covariation varies over the course of the season

Correlation networks showing patterns of covariation within and between phenotyping modalities. Nodes of the network are connected if they are significantly correlated (Pearson, FDR; p.adj < 0.05). Edge thickness is proportional to the strength of correlation (multiplied by 16 for visibility). Edge color reflects the direction of the correlation where blue edges indicate positive correlations and orange edges indicate negative correlations. Modalities are indicated by a leading character and node color: ionomics (iPCs; purple), metabolomics (mPCs; pink), gene expression (gPCs; yellow), leaf shape (sPCs; green). Network topologies are shown for **(A)** anthesis, **(B)** veraison, and **(C)** harvest.

Figure Supplement Legends:

Supplemental Figure 1: Experimental Design

(A) Vineyard Map. The vineyard features a randomized block design where 'Chambourcin' is grown ungrafted and grafted to three rootstock genotypes: '1103P', '3309C', and 'SO4'. Each row is treated with one of three irrigation treatments: full replacement of ET, reduced-deficit, no replacement of ET. Each cell of the vineyard contains four replicate grafts. **(B)** Phenotype sampling scheme across the four replicates in a cell. All vines (288) were sampled for ionomics and leaf shape. The middle two vines in the front half of the vineyard (72) were additionally sampled for metabolomics, gene expression, and physiology. **(C)** Phenotype sample scheme within a vine (along a shoot). For each plant, young leaves were sampled for ionomics, leaf shape, and gene expression. Middle leaves were sampled for ionomics, leaf shape, metabolomics, and physiology. Older leaves were sampled for ionomics and leaf shape. Samples for ionomics and leaf shape were taken from the same shoot. All other phenotypes were sampled from independent shoots. **(D)** Rootstock relatedness. Each of the rootstocks in this trial shares a parent species with a different rootstock. '1103P' is a cross between *Vitis rupestris* and *V. berlandieri*. '3309C' is a cross between *V. rupestris* and *V. riparia*. 'SO4' is a cross between *V. riparia* and *V. berlandieri*. The parent that is shared between each pair of rootstocks is highlighted. This figure is partially reproduced from [19] available under a Creative Common license (CC BY 4.0).

Supplemental Figure 2: Patterns of ion covariation change over experimental treatments

Correlation networks showing patterns of ion covariation across phenological stages and shoot position. Nodes of the network are connected if they are significantly correlated (Pearson, FDR; p.adj < 0.05). Edge thickness is proportional to the strength of correlation (multiplied by 16 for visibility). Edge color reflects the direction of the correlation where blue edges indicate positive correlations and orange edges indicate negative correlations.

Supplemental Figure 3: Patterns of variation contributing to gene expression linear discriminants

(**A**) Projections of leaf gene expression samples into the first two dimensions of a linear discriminant space trained to maximize variation between phenological stages, rows in the vineyard, and rootstock genotype. For each LD, the PCs that loaded significantly (>1.96 sd from the mean loading) are listed in order of loading magnitude. (**B**) Distribution of the top loading PCs onto LD1 and LD2 for each of the trained models.

Supplemental Figure 4: Patterns of variation in leaf shape are subtle

(**A**) Percent variation captured in linear models fit to each of the top 20 principal components of leaf morphology. Presence of a cell indicates the model term (top) was significant for that PC (left, percent variation explained by the PC in parentheses). (**B**) Composite leaf traces for the main rootstock genotype effect identified on PC1.

Supplemental Figure 5: Example correlations within and between data modalities over the course of the season

(**A**) Example correlation showing a strong within-modality correlation between the ionomics gPC1 and gPC2 at anthesis. Pearson correlations by phenological stage and CIs derived from 10000 random 90% draws are shown for each panel. Generally speaking, CIs overlapping with 0 were not accepted as significant. (**B**) Example correlation showing one of the stronger between-modality correlations between the gene expression gPC4 and morphology (shape) sPC3 at veraison. (**C**) Example correlation of a relationship that is present multiple times over the course of the season between metabolomics mPC3 and gene expression gPC6 at both veraison and harvest. (**D**) Example correlation that is dynamic over the course of the growing season between the ionomics mPC3 and mPC6.

Supplemental Figure 6: Trait covariation varies over rootstock genotype

Correlation networks showing patterns of covariation within and between phenotyping modalities. Nodes of the network are connected if they are significantly correlated (Pearson, FDR; p.adj < 0.05). Edge thickness is proportional to the strength of correlation (multiplied by 16 for visibility). Edge color reflects the direction of the correlation where blue edges indicate positive correlations and orange edges indicate negative correlations. Modalities are indicated by a leading character and node color: ionomics (iPCs; purple), metabolomics (mPCs; pink), gene expression (gPCs; yellow), leaf shape (sPCs; green). Network topologies are shown for **(A)** Ungrafted, **(B)** '1103P'-grafted vines, **(C)** '3309C'-grafted vines, and **(D)** 'SO4'-grafted vines.

Availability of Data:

Ionomics data are available at https://dx.doi.org/10.6084/m9.figshare.13200980 . Metabolomics data are available at https://dx.doi.org/10.6084/m9.figshare.13201043. Gene expression data are available in the Sequence Read Archive under BioProject PRJNA674915. Leaf scans and leaf landmarks are available at https://dx.doi.org/10.6084/m9.figshare.13200953. Weather and physiology data are available at https://dx.doi.org/10.6084/m9.figshare.13198682 and https://dx.doi.org/10.6084/m9.figshare.13201016, respectively.

Availability of Code:

All code for this paper including shell scripts for RNAseq analysis and Jupyter Notebooks for data analysis in R can be found on the Vitis Underground GitHub (https://github.com/PGRP1546869/mt_vernon_2017_leaf).

Author Contributions:

AJM, DHC, AF, LGK, MK, JPL, and QM designed the experiment. ZNH, LLK, MA, JFS, ZM, NB, EF, and JPL contributed to sample collection and sample processing. ZNH, LLK, JFS, and MA contributed to

data analysis. ZNH and AJM contributed to the writing of the manuscript. All authors contributed to manuscript editing.

References:

1. Gehan MA, Fahlgren N, Abbasi A, Berry JC, Callen ST, Chavez L, et al.. PlantCV v2: Image analysis software for high-throughput plant phenotyping. *PeerJ*. 2017; doi: 10.7717/peerj.4088.

2. Ubbens JR, Stavness I. Deep Plant Phenomics: A Deep Learning Platform for Complex Plant Phenotyping Tasks. *Front Plant Sci*. 2017; doi: 10.3389/fpls.2017.01190.

3. Ubbens J, Cieslak M, Prusinkiewicz P, Stavness I. Latent Space Phenotyping: Automatic Image-Based Phenotyping for Treatment Studies.

4. Soulé M. PHENETICS OF NATURAL POPULATIONS I. PHENETIC RELATIONSHIPS OF INSULAR POPULATIONS OF THE SIDE-BLOTCHED LIZARD. *Evolution*. 1967; doi: 10.1111/j.1558-5646.1967.tb03413.x.

5. Houle D, Govindaraju DR, Omholt S. Phenomics: the next challenge. *Nat Rev Genet*. 2010; doi: 10.1038/nrg2897.

6. Mudge K, Janick J, Scofield S, Goldschmidt EE. A History of Grafting. In: Janick J, editor. *Horticultural Reviews*. Hoboken, NJ, USA: John Wiley & Sons, Inc.;

7. Pouget R. Histoire de la lutte contre le phylloxéra de la vigne en France: 1868-1895. *Hist Sci Med*. INRA; 1990;

8. Walker MA, Lund K, Agüero C, Riaz S, Fort K, Heinitz C, et al.. BREEDING GRAPE ROOTSTOCKS FOR RESISTANCE TO PHYLLOXERA AND NEMATODES - IT'S NOT ALWAYS EASY. Acta Horticulturae.

9. Warschefsky EJ, Klein LL, Frank MH, Chitwood DH, Londo JP, von Wettberg EJB, et al.. Rootstocks: Diversity, Domestication, and Impacts on Shoot Phenotypes. *Trends Plant Sci*. Elsevier Current Trends; 2016; doi: 10.1016/j.tplants.2015.11.008.

10. Tramontini S, Vitali M, Centioni L, Schubert A, Lovisolo C. Rootstock control of scion response to water stress in grapevine. Environmental and Experimental Botany.

11. Bavaresco L, Lovisolo C. Effect of grafting on grapevine chlorosis and hydraulic conductivity. *VITIS-Journal of Grapevine Research*. Citeseer; 2015;

12. Ferlito F, Distefano G, Gentile A, Allegra M, Lakso AN, Nicolosi E. Scion–rootstock interactions influence the growth and behaviour of the grapevine root system in a heavy clay soil. Australian Journal of Grape and Wine Research.

13. Ordish G. The great wine blight. J.M. Dent & Sons;

14. Cookson SJ, Ollat N. Grafting with rootstocks induces extensive transcriptional re-programming in the shoot apical meristem of grapevine. *BMC Plant Biol*. BioMed Central; 2013; doi: 10.1186/1471-2229-13-147.

15. Corso M, Vannozzi A, Ziliotto F, Zouine M, Maza E, Nicolato T, et al.. Grapevine Rootstocks Differentially Affect the Rate of Ripening and Modulate Auxin-Related Genes in Cabernet Sauvignon Berries. *Front Plant Sci*. Frontiers; 2016; doi: 10.3389/fpls.2016.00069.

16. Berdeja M, Nicolas P, Kappel C, Dai ZW, Hilbert G, Peccoux A, et al.. Water limitation and rootstock genotype interact to alter grape berry metabolism through transcriptome reprogramming. *Hortic Res*. 2015; doi: 10.1038/hortres.2015.12.

17. Zombardo A, Crosatti C, Bagnaresi P, Bassolino L, Reshef N, Puccioni S, et al.. Transcriptomic and biochemical investigations support the role of rootstock-scion interaction in grapevine berry quality. *BMC*

795 *Genomics*. 2020; doi: 10.1186/s12864-020-06795-5.

796 18. Chitarra W, Perrone I, Avanzato CG, Minio A, Boccacci P, Santini D, et al.. Grapevine Grafting:
797 Scion Transcript Profiling and Defense-Related Metabolites Induced by Rootstocks. *Front Plant Sci*.
798 Frontiers; 2017; doi: 10.3389/fpls.2017.00654.

799 19. Migicovsky Z, Harris ZN, Klein LL, Li M, McDermaid A, Chitwood DH, et al.. Rootstock effects on
800 scion phenotypes in a "Chambourcin" experimental vineyard. *Horticulture Research*. Nature Publishing
801 Group; 2019; doi: 10.1038/s41438-019-0146-2.

802 20. Galet P. A Practical Ampelography: Grapevine Identification. Comstock Pub. Associates;

803 21. Mullins MG, Bouquet A, Williams LE. Biology of the Grapevine. Cambridge University Press;

804 22. Chitwood DH, Ranjan A, Martinez CC, Headland LR, Thiem T, Kumar R, et al.. A modern
805 ampelography: a genetic basis for leaf shape and venation patterning in grape. *Plant Physiol*. 2014; doi:
806 10.1104/pp.113.229708.

807 23. Chitwood DH, Klein LL, O'Hanlon R, Chacko S, Greg M, Kitchen C, et al.. Latent developmental
808 and evolutionary shapes embedded within the grapevine leaf. New Phytologist.

809 24. Klein LL, Caito M, Chapnick C, Kitchen C, O'Hanlon R, Chitwood DH, et al.. Digital Morphometrics
810 of Two North American Grapevines (Vitis: Vitaceae) Quantifies Leaf Variation between Species, within
811 Species, and among Individuals. *Front Plant Sci*. 2017; doi: 10.3389/fpls.2017.00373.

812 25. Grimes DW, Williams LE. Irrigation Effects on Plant Water Relations and Productivity of Thompson
813 Seedless Grapevines. *Crop Sci*. 1990; doi: 10.2135/cropsci1990.0011183X003000020003x.

814 26. Williams LE, Grimes DW. Modelling vine growth-development of a data set for a water balance
815 subroutine. *Proceedings of the Sixth Australian Wine Industry Technical Conference*. p. 169–74.

816 27. Gautier A, Cookson SJ, Lagalle L, Ollat N, Marguerit E. Influence of the three main genetic
817 backgrounds of grapevine rootstocks on petiolar nutrient concentrations of the scion, with a focus on
818 phosphorus. *OENO One*. 2020; doi: 10.20870/oeno-one.2020.54.1.2458.

819 28. Lecourt J, Lauvergeat V, Ollat N, Vivin P, Cookson SJ. Shoot and root ionome responses to nitrate
820 supply in grafted grapevines are rootstock genotype dependent: Rootstock and nitrogen supply affect
821 grapevine ionome. *Aust J Grape Wine Res*. 2015; doi: 10.1111/ajgw.12136.

822 29. Salt DE, Baxter I, Lahner B. Ionomics and the study of the plant ionome. *Annu Rev Plant Biol*. 2008;
823 doi: 10.1146/annurev.arplant.59.032607.092942.

824 30. Baxter I. Ionomics: The functional genomics of elements. *Brief Funct Genomics*. 2010; doi:
825 10.1093/bfgp/elp055.

826 31. Ziegler G, Terauchi A, Becker A, Armstrong P, Hudson K, Baxter I. Ionomic Screening of Field-
827 Grown Soybean Identifies Mutants with Altered Seed Elemental Composition. The Plant Genome.

828 32. Oliver SG, Winson MK, Kell DB, Baganz F. Systematic functional analysis of the yeast genome.
829 *Trends Biotechnol*. 1998; doi: 10.1016/s0167-7799(98)01214-1.

830 33. Tweeddale H, Notley-McRobb L, Ferenci T. Effect of slow growth on metabolism of Escherichia coli,
831 as revealed by global metabolite pool ("metabolome") analysis. *J Bacteriol*. 1998; doi:
832 10.1128/JB.180.19.5109-5116.1998.

833 34. Islam MN, Downey F, Ng CKY. Comparative analysis of bioactive phytochemicals from Scutellaria
834 baicalensis, Scutellaria lateriflora, Scutellaria racemosa, Scutellaria tomentosa and Scutellaria wrightii by
835 LC-DAD-MS. *Metabolomics*. Springer; 7:446–532011;

836 35. Tautenhahn R, Patti GJ, Rinehart D, Siuzdak G. XCMS Online: a web-based platform to process
837 untargeted metabolomic data. *Anal Chem*. 2012; doi: 10.1021/ac300698c.

838 36. Tandonnet S, Torres TT. Traditional versus 3' RNA-seq in a non-model species. *Genom Data*. 2017;
839 doi: 10.1016/j.gdata.2016.11.002.

840 37. Bolger AM, Lohse M, Usadel B. Trimmomatic: a flexible trimmer for Illumina sequence data.
841 *Bioinformatics*. 2014; doi: 10.1093/bioinformatics/btu170.

842 38. Bushnell B. BBTools software package. *URL http://sourceforge net/projects/bbmap*. 2017;

843 39. Jaillon O, Aury J-M, Noel B, Policriti A, Clepet C, Casagrande A, et al.. The grapevine genome
844 sequence suggests ancestral hexaploidization in major angiosperm phyla. *Nature*. 2007; doi:
845 10.1038/nature06148.

846 40. Canaguier A, Grimplet J, Di Gaspero G, Scalabrin S, Duchêne E, Choisne N, et al.. A new version of
847 the grapevine reference genome assembly (12X.v2) and of its annotation (VCost.v3). *Genom Data*. 2017;
848 doi: 10.1016/j.gdata.2017.09.002.

849 41. Dobin A, Davis CA, Schlesinger F, Drenkow J, Zaleski C, Jha S, et al.. STAR: ultrafast universal
850 RNA-seq aligner. *Bioinformatics*. 2013; doi: 10.1093/bioinformatics/bts635.

851 42. Anders S, Pyl PT, Huber W. HTSeq: Analysing high-throughput sequencing data with Python.

852 43. Love MI, Huber W, Anders S. Moderated estimation of fold change and dispersion for RNA-seq data
853 with DESeq2. *Genome Biol*. 2014; doi: 10.1186/s13059-014-0550-8.

854 44. Anders S, Huber W. Differential expression analysis for sequence count data. *Genome Biol*. 2010;
855 doi: 10.1186/gb-2010-11-10-r106.

856 45. Dryden IL, Mardia KV. Statistical Shape Analysis: With Applications in R. John Wiley & Sons;

857 46. Degu A, Hochberg U, Sikron N, Venturini L, Buson G, Ghan R, et al.. Metabolite and transcript
858 profiling of berry skin during fruit development elucidates differential regulation between Cabernet

Sauvignon and Shiraz cultivars at branching points in the polyphenol pathway. *BMC Plant Biol*. 2014; doi: 10.1186/s12870-014-0188-4.

47. Anesi A, Stocchero M, Dal Santo S, Commisso M, Zenoni S, Ceoldo S, et al.. Towards a scientific interpretation of the terroir concept: plasticity of the grape berry metabolome. *BMC Plant Biol*. 2015; doi: 10.1186/s12870-015-0584-4.

48. Cuadros-Inostroza A, Ruíz-Lara S, González E, Eckardt A, Willmitzer L, Peña-Cortés H. GC-MS metabolic profiling of Cabernet Sauvignon and Merlot cultivars during grapevine berry development and network analysis reveals a stage- and cultivar-dependent connectivity of primary metabolites. *Metabolomics*. 2016; doi: 10.1007/s11306-015-0927-z.

49. Dal Santo S, Fasoli M, Negri S, D'Incà E, Vicenzi N, Guzzo F, et al.. Plasticity of the Berry Ripening Program in a White Grape Variety. *Front Plant Sci*. 2016; doi: 10.3389/fpls.2016.00970.

50. Zamboni A, Di Carli M, Guzzo F, Stocchero M, Zenoni S, Ferrarini A, et al.. Identification of putative stage-specific grapevine berry biomarkers and omics data integration into networks. *Plant Physiol*. 2010; doi: 10.1104/pp.110.160275.

51. Dal Santo S, Tornielli GB, Zenoni S, Fasoli M, Farina L, Anesi A, et al.. The plasticity of the grapevine berry transcriptome. *Genome Biol*. 2013; doi: 10.1186/gb-2013-14-6-r54.

52. Chitwood DH, Rundell SM, Li DY, Woodford QL, Yu TT, Lopez JR, et al.. Climate and Developmental Plasticity: Interannual Variability in Grapevine Leaf Morphology. *Plant Physiol*. 2016; doi: 10.1104/pp.15.01825.

53. Chitwood DH, Mullins J, Migicovsky Z, Frank M, VanBuren R, Londo JP. Vein-to-blade ratio is an allometric indicator of climate-induced changes in grapevine leaf size and shape. bioRxiv.

54. Gautier A, Cookson SJ, Lagalle L, Ollat N, Marguerit E. Influence of the three main genetic

backgrounds of grapevine rootstocks on petiolar nutrient concentrations of the scion, with a focus on phosphorus. *OENO One*. 2020; doi: 10.20870/oeno-one.2020.54.1.2458.

55. Canas S, Assunção M, Brazão J, Zanol G, Eiras-Dias JE. Phenolic compounds involved in grafting incompatibility of Vitis spp: development and validation of an analytical method for their quantification. *Phytochem Anal*. 2015; doi: 10.1002/pca.2526.

56. Prodhomme D, Valls Fonayet J, Hévin C, Franc C, Hilbert G, de Revel G, et al.. Metabolite profiling during graft union formation reveals the reprogramming of primary metabolism and the induction of stilbene synthesis at the graft interface in grapevine. *BMC Plant Biol*. 2019; doi: 10.1186/s12870-019-2055-9.

57. Vitulo N, Forcato C, Carpinelli EC, Telatin A, Campagna D, D'Angelo M, et al.. A deep survey of alternative splicing in grape reveals changes in the splicing machinery related to tissue, stress condition and genotype. *BMC Plant Biol*. 2014; doi: 10.1186/1471-2229-14-99.

58. Harris ZN, Kovacs LG, Londo JP. RNA-seq-based genome annotation and identification of long-noncoding RNAs in the grapevine cultivar "Riesling." *BMC Genomics*. BioMed Central; 18:9372017;

59. Williams BR, Edwards CE, Kwasniewski MT, Miller AJ. Epigenomic patterns reflect irrigation and grafting in the grapevine clone'Chambourcin'. *bioRxiv*. Cold Spring Harbor Laboratory; 2020;

60. Marasco R, Rolli E, Fusi M, Michoud G, Daffonchio D. Grapevine rootstocks shape underground bacterial microbiome and networking but not potential functionality. *Microbiome*. 2018; doi: 10.1186/s40168-017-0391-2.

61. Swift JF, Hall ME, Harris ZN, Kwasniewski MT, Miller AJ. Grapevine microbiota reflect diversity among compartments and complex interactions within and among root and shoot systems. bioRxiv.

62. Palumbo MC, Zenoni S, Fasoli M, Massonnet M, Farina L, Castiglione F, et al.. Integrated network

903 analysis identifies fight-club nodes as a class of hubs encompassing key putative switch genes that induce
904 major transcriptome reprogramming during grapevine development. *Plant Cell*. Am Soc Plant Biol;
905 26:4617–352014;

906 63. Savoi S, Wong DCJ, Arapitsas P, Miculan M, Bucchetti B, Peterlunger E, et al.. Transcriptome and
907 metabolite profiling reveals that prolonged drought modulates the phenylpropanoid and terpenoid
908 pathway in white grapes (Vitis vinifera L.). *BMC Plant Biol*. 2016; doi: 10.1186/s12870-016-0760-1.

909 64. Savoi S, Wong DCJ, Degu A, Herrera JC, Bucchetti B, Peterlunger E, et al.. Multi-Omics and
910 Integrated Network Analyses Reveal New Insights into the Systems Relationships between Metabolites,
911 Structural Genes, and Transcriptional Regulators in Developing Grape Berries (Vitis vinifera L.) Exposed
912 to Water Deficit. *Front Plant Sci*. 2017; doi: 10.3389/fpls.2017.01124.

913 65. Wong DCJ, Matus JT. Constructing Integrated Networks for Identifying New Secondary Metabolic
914 Pathway Regulators in Grapevine: Recent Applications and Future Opportunities. *Front Plant Sci*. 2017;
915 doi: 10.3389/fpls.2017.00505.

916 66. Fabres PJ, Collins C, Cavagnaro TR, Rodríguez López CM. A Concise Review on Multi-Omics Data
917 Integration for Terroir Analysis in Vitis vinifera. *Front Plant Sci*. 2017; doi: 10.3389/fpls.2017.01065.

918 67. Huang S, Chaudhary K, Garmire LX. More Is Better: Recent Progress in Multi-Omics Data
919 Integration Methods. *Front Genet*. 2017; doi: 10.3389/fgene.2017.00084.

920 68. Stein-O'Brien GL, Arora R, Culhane AC, Favorov AV, Garmire LX, Greene CS, et al.. Enter the
921 Matrix: Factorization Uncovers Knowledge from Omics. *Trends Genet*. 2018; doi:
922 10.1016/j.tig.2018.07.003.

923 69. Fox J, Friendly M, Weisberg S. Hypothesis tests for multivariate linear models using the car package.
924 *R J*. Citeseer; 5:39–522013;

925 70. R Core Team. R: A language and environment for statistical computing. Vienna, Austria;

926 71. Lenth R, Singmann H, Love J, Others. Emmeans: Estimated marginal means, aka least-squares
927 means. *R package version*. 12018;

928 72. Ripley BD. Modern applied statistics with S. Springer;

929 73. Wickham H. ggplot2: Elegant Graphics for Data Analysis. Springer;

930 74. Liaw A, Wiener M, Others. Classification and regression by randomForest. *R news*. 2:18–222002;

931 75. Kuhn M. Predictive Modeling with R and the caret Package. *Google Scholar*. 2013;

932 76. Team RC, Others. R foundation for statistical computing. *Vienna, Austria*. 32013;

933 77. Csardi G, Nepusz T, Others. The igraph software package for complex network research.
934 *InterJournal, complex systems*. 1695:1–92006;

935

Figure 1

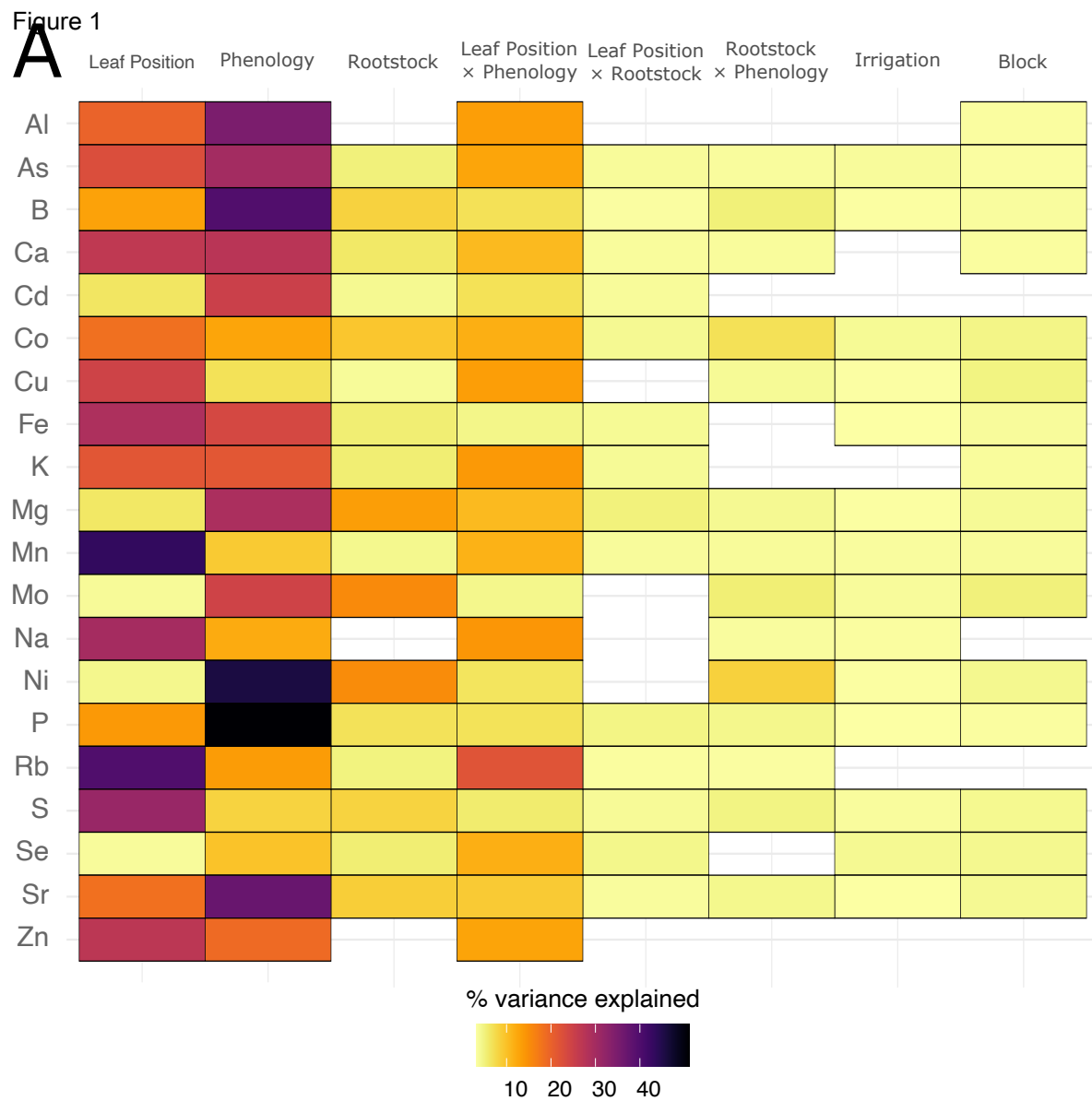

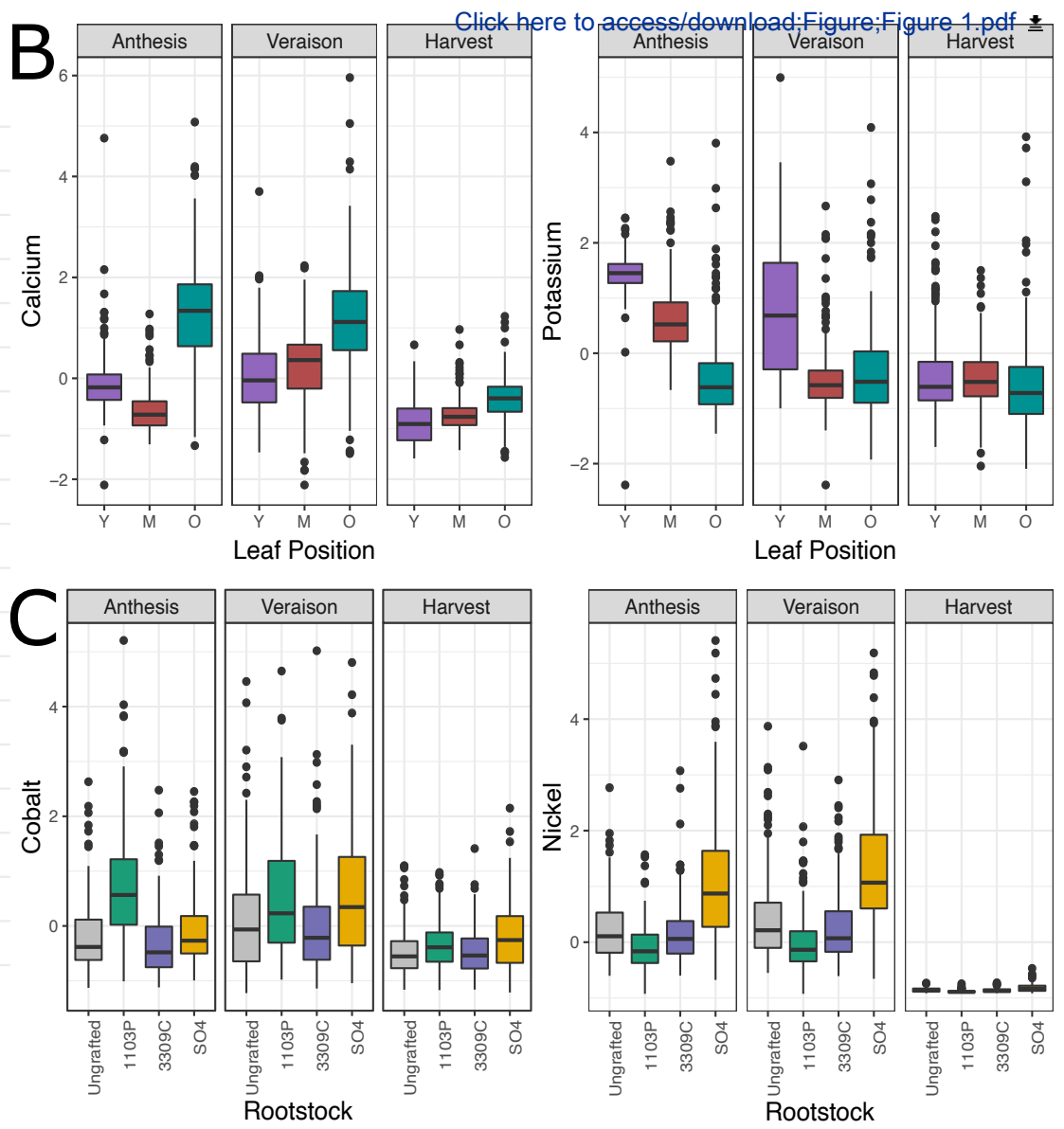

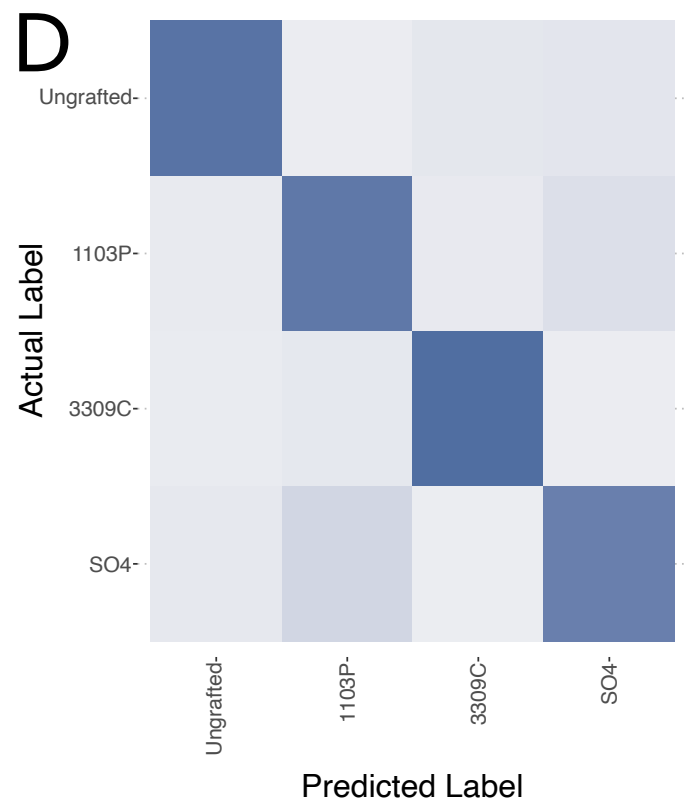

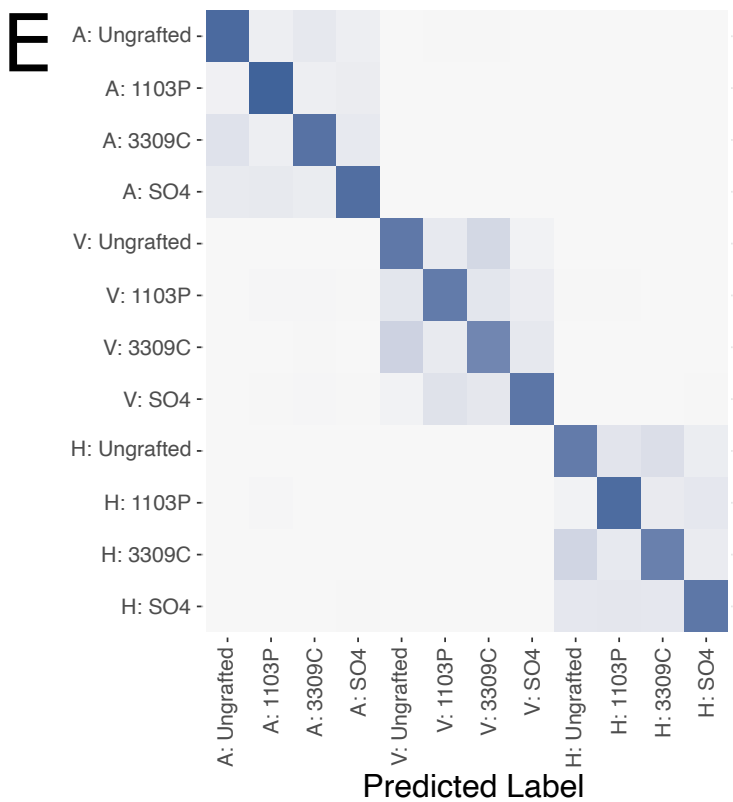

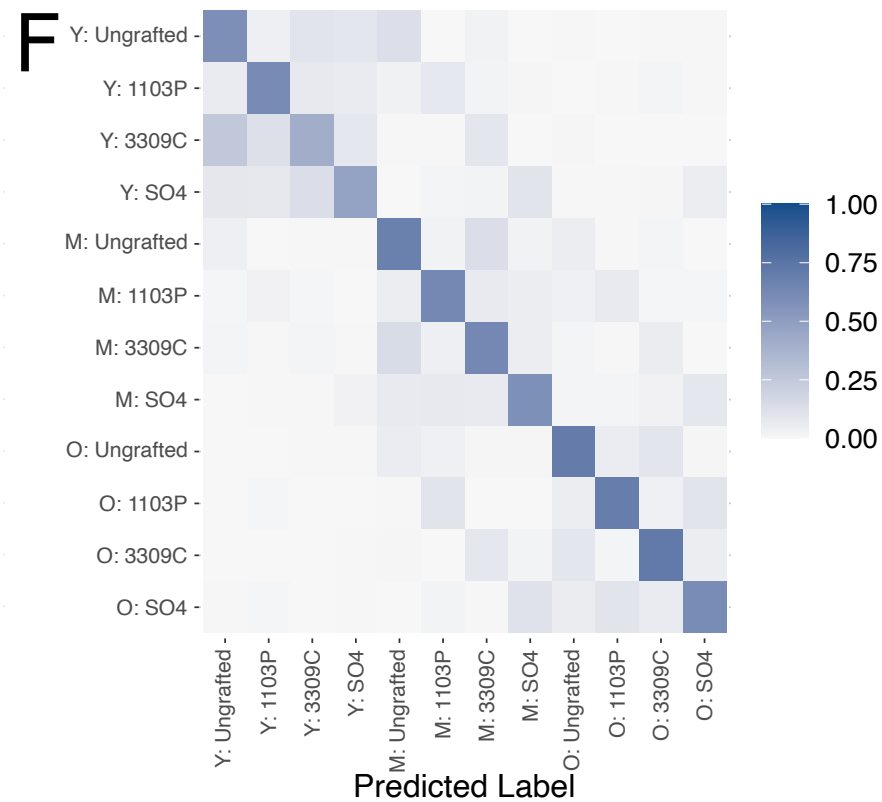

Figure 2

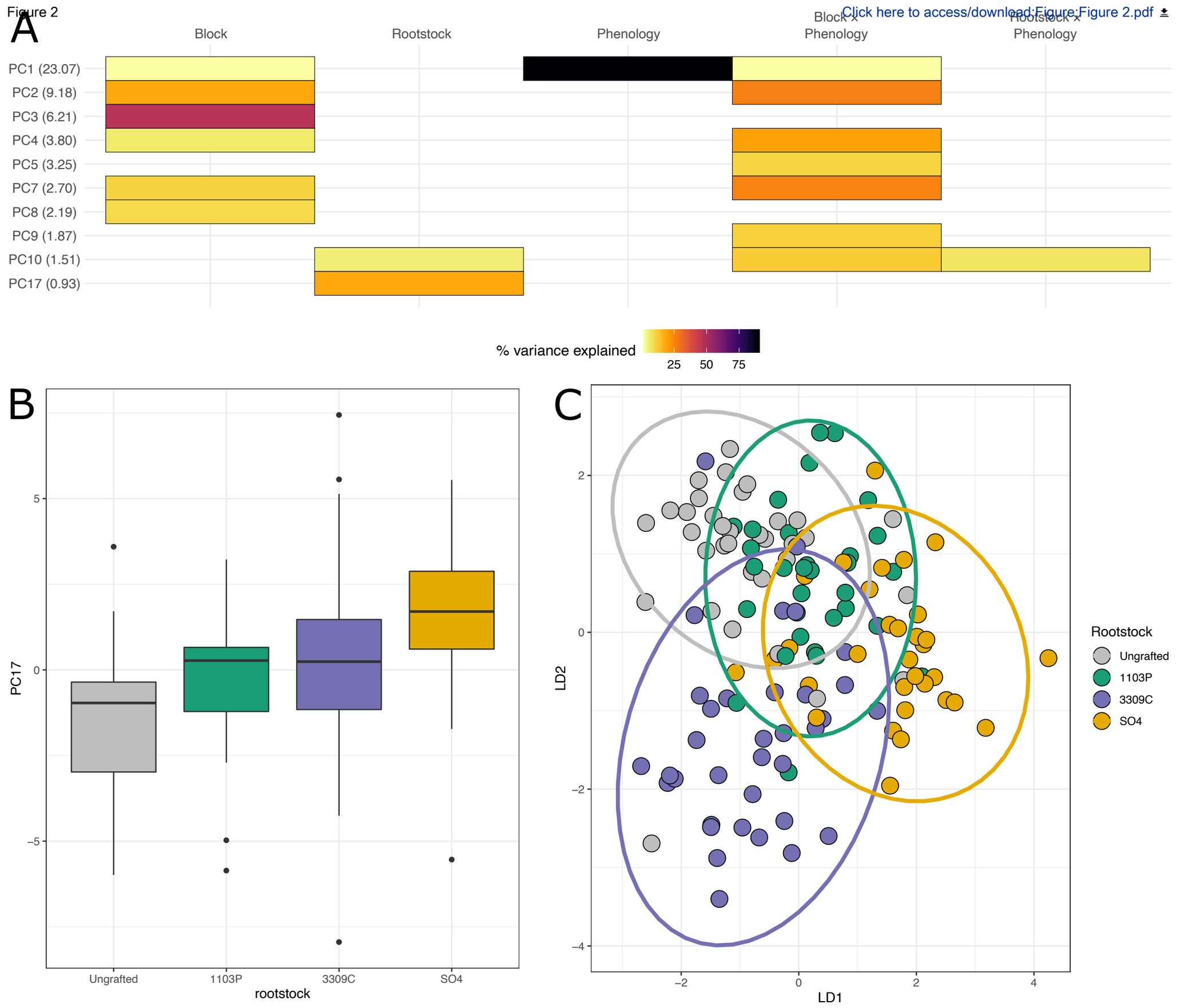

Figure 3

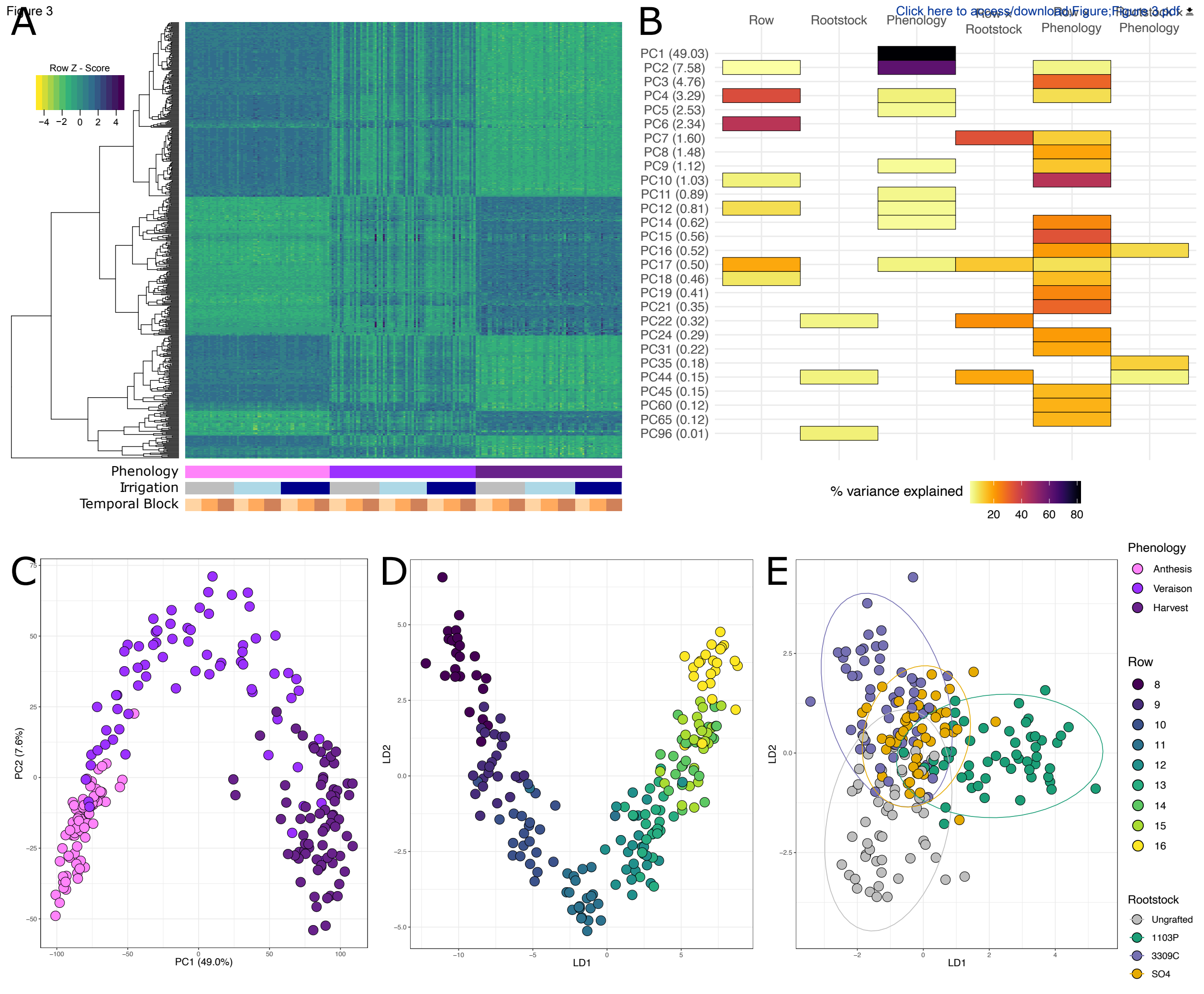
A
Row Z - Score
−4 −2 0 2 4
Phenology
Irrigation
Temporal Block
B
Row
Rootstock
Phenology
Row x Rootstock
Row x Phenology
Rootstock x Phenology
PC1 (49.03)
PC2 (7.58)
PC3 (4.76)
PC4 (3.29)
PC5 (2.53)
PC6 (2.34)
PC7 (1.60)
PC8 (1.48)
PC9 (1.12)
PC10 (1.03)
PC11 (0.89)
PC12 (0.81)
PC14 (0.62)
PC15 (0.56)
PC16 (0.52)
PC17 (0.50)
PC18 (0.46)
PC19 (0.41)
PC21 (0.35)
PC22 (0.32)
PC24 (0.29)
PC31 (0.22)
PC35 (0.18)
PC44 (0.15)
PC45 (0.15)
PC60 (0.12)
PC65 (0.12)
PC96 (0.01)
% variance explained
20 40 60 80
C
PC2 (7.6%)
PC1 (49.0%)
D
LD2
LD1
E
LD2
LD1
Phenology
Anthesis
Veraison
Harvest
Row
8
9
10
11
12
13
14
15
16
Rootstock
Ungrafted
1103P
3309C
SO4

Figure 4

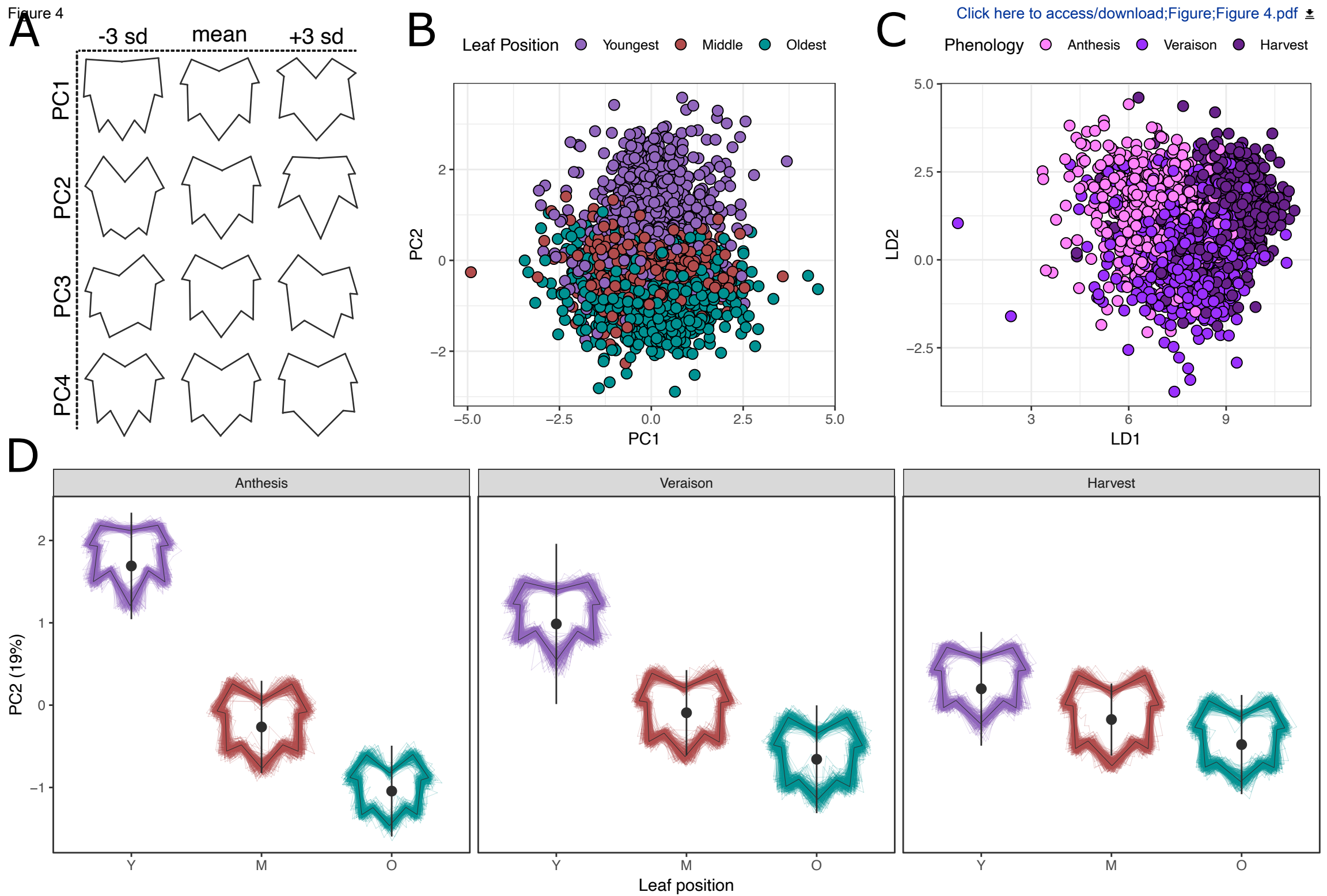

Figure 5

Click here to access/download;Figure;Figure 5.pdf

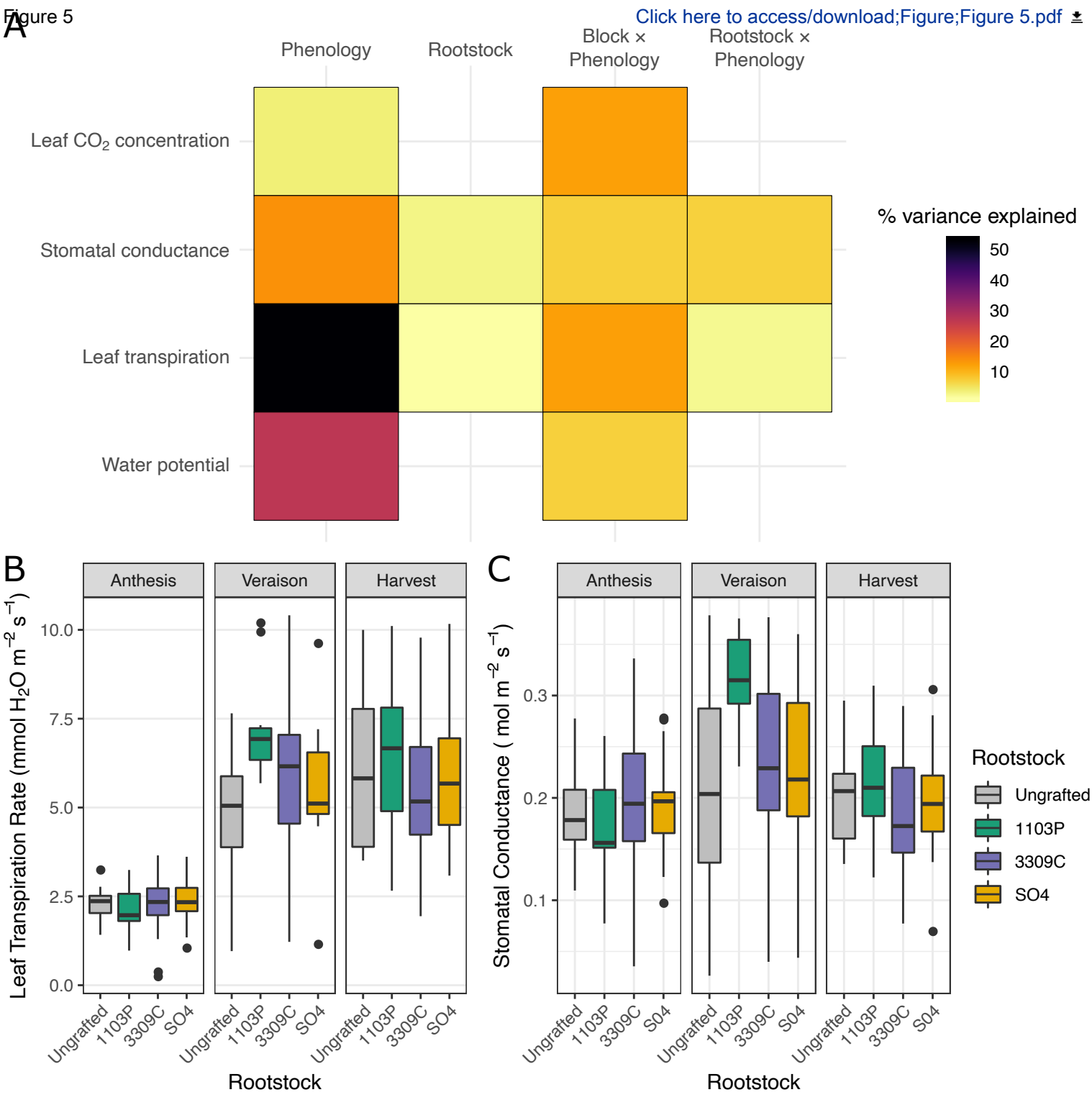

Figure 6

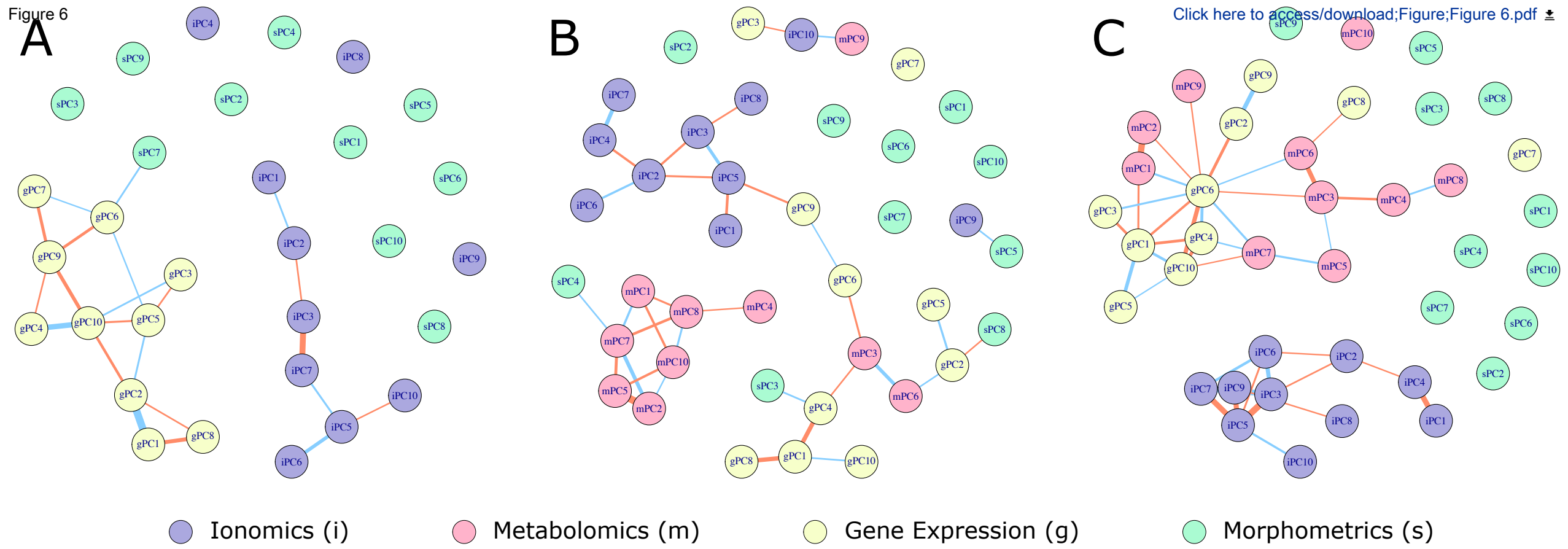

Click here to access/download;Figure;Figure 6.pdf

Supplemental Figure 1

Supplemental Figure 2

Supplemental Figure 3

Supplemental Figure 4

Supplemental Figure 5

Supplemental Figure 6

Dear Editorial Board,

We are excited to submit our manuscript entitled "Multi-dimensional leaf phenotypes reflect root system genotype in grafted grapevine over the growing season" to be considered for peer review at *GigaScience*. Our manuscript describes advances in the fundamental question of how phenotypic variation changes over time in perennial plants, focusing primarily on the influence of below-ground organs on above-ground phenotypes using multi-dimensional phenomic platforms. We believe our manuscript matches the journal's focus on using big data in the life sciences and to ensure reproducibility through extensive data and analytical transparency; further, our work fits nicely within the thematic series on Plant Phenomics. We note that our work has been uploaded as a preprint on BioRxiv: https://www.biorxiv.org/content/10.1101/2020.11.10.376947v1.abstract

In plants, understanding how the root system affects above-ground structures of the shoot system is a fundamental question in plant biology. Grafting offers a powerful experimental approach where clonally propagated genotypes are fused to form grafted individuals with genetically distinct root and shoot systems. Populations generated via grafting can include replicated individuals with genetically identical shoot systems but genetically distinct root systems. This allows for quantification of phenotypic variation expressed in the shoot system as a function of root system genotype. Our study quantifies root system influence on shoot system phenotypes in grafted grapevines through comprehensive phenotyping of leaves, the primary site of photosynthesis and important markers of cultivar identification. In an experimental grafted vineyard in southwestern Missouri, we surveyed five multi-dimensional phenotyping modalities in leaves at three time points in the season: ionomics, metabolomics, transcriptomics, morphometrics (shape), and physiology. These data were used to address the broad questions: to what extent do root system genotypes influence leaf phenotypes, and how does this change over the course of a season?

To our knowledge, this work is the largest study of its kind both in the size of the population (a ten-year old experimental vineyard with four root-shoot combinations replicated 72 times in a randomized block design of 288 vines) and the depth to which we surveyed leaf phenotypes (five multi-dimensional phenotyping modalities at three time points throughout a season). This robust study design in addition to the application of multi-dimensional phenotyping platforms allowed us to identify the complex nature by which root systems can influence shoot system phenotypes.

Work presented here demonstrates that the root system exercises subtle but ubiquitous influence on leaves for every phenotypic modality examined. Moreover, our work highlights the dynamic nature of root-shoot interactions: root system influence on leaf phenotypes changes over the course of a season, with the most dramatic effects observed during early season growth, but with distinct patterns observed across modalities. In addition, we show that covariation among multi-dimensional leaf phenotypes is highly dynamic across the rootstock genotype and time of season.

We appreciate your time and consideration of our manuscript. We look forward to hearing from you.

Best regards,
Zachary N. Harris & Allison J. Miller